https://doi.org/10.5194/egusphere-2026-2662
Preprint. Discussion started: 29 May 2026

Atmospheric methane growth rates, 2018-2024, driven mainly by emission changes but atmospheric photochemistry is important

Liang Feng[1,2,*], Paul I. Palmer[1,2,*], Haolin Wang[2], Robert Parker[3,4], Hartmut Boesch[5], Sébastien C. Biraud[6], Łukasz Chmura[7,8], Emanuel Gloor[9], László Haszpra[10], Elena Kozlova[11], Euan G. Nisbet[12], Steffen M. Noe[13], Thomas Röckmann[14], Rodrigo Augusto Ferreira de Souza[15], Martin Steinbacher[16],

1. National Centre for Earth Observation, University of Edinburgh, Edinburgh, UK
2. School of GeoSciences, University of Edinburgh, Edinburgh, UK
3. National Centre for Earth Observation, Space Park Leicester, University of Leicester, Leicester, UK
4. Earth Observation Science, School of Physics and Astronomy, University of Leicester, Leicester, UK
5. Institute of Environmental Physics, University of Bremen, Bremen, Germany
6. Climate and Ecosystem Sciences Division, Lawrence Berkeley National Laboratory, Berkeley, CA, USA
7. AGH University of Krakow, Faculty of Physics and Applied Computer Science, Krakow, Poland
8. Institute of Meteorology and Water Management, National Research Institute, Warsaw, Poland
9. School of Geography, University of Leeds, Leeds, UK
10. Institute for Marine and Atmospheric research Utrecht (IMAU), Utrecht University, Utrecht, Netherlands
11. College of Life and Environmental Sciences, University of Exeter, Exeter, UK
12. Department of Earth Sciences, Royal Holloway, University of London, London, UK
13. Institute of Forestry and Engineering, Estonian University of Life Sciences, Tartu, Estonia
14. Institute for Nuclear Research (ATOMKI), Debrecen, Hungary
15. School of Technology, University of the State of Amazonas (UEA), Manaus, AM, Brazil
16. Swiss Federal Laboratories for Materials Science and Technology (EMPA), Dübendorf, Switzerland

Correspondence to: Liang Feng (liang.feng@staffmail.ed.ac.uk) and Paul I. Palmer (pip@ed.ac.uk)

Abstract. Global atmospheric methane growth rate has increased dramatically since 2007, peaking in 2021, yet the relative roles of emissions and atmospheric oxidation remain uncertain. Accurate attribution is essential for climate mitigation because emissions-driven and chemistry-driven changes imply fundamentally different policy responses. Here we investigate global methane production and loss from 2018 to 2024 using an ensemble Kalman filter coupled to the GEOS-Chem chemical transport model. We employ two methane inversion configurations: assuming climatological monthly OH distributions or jointly optimizing zonal mean OH with methane. The joint inversion reveals substantial interannual variability in OH, including an ~18% decline in 2020 followed by a recovery in subsequent years. Accounting for this variability reduces the inferred 2019–2020 emission increase by ~63% (14±6 Tg/yr versus 37±5.5 Tg/yr with fixed OH), demonstrating that changes in OH strongly influences source attribution. The total increased methane loss, 2024 minus 2019, is about 31±6 Tg/yr, including a temperature-driven increase of the OH+methane reaction rate that represents more than 40% (~14 Tg/yr) of the total sink increase. Most of the sink variations originate from the tropics, where the largest shifts in emission occur. Despite year-to-year variations, emissions remain the primary driver of changes in the methane growth rate change, except in 2020. Both inversions identify significant emission reductions over tropical South America in 2023–2024, likely linked to regional

https://doi.org/10.5194/egusphere-2026-2662
Preprint. Discussion started: 29 May 2026

drought. Broadly, our results underscore the necessity of jointly estimating methane sources and sinks to interpret recent atmospheric methane trends so that appropriate policy interventions can be identified.

1 Introduction

Atmospheric methane is undergoing a surge unlike anything in the recent geologic record. In 2024, the global annual mean methane level reached 1945.47±0.61 ppbv – 17% higher than when systematic measurements began in 1984, more than 2.5 times preindustrial levels (WMO, 2025; Lan et al., 2026), and unmatched for at least 800,000 years (Loulergue et al., 2008). Despite it being approximately 200 times more dilute in the atmosphere than CO_2, methane is responsible for about a third of a current warming (IPCC AR6, Calvin et al., 2023). Because methane warms the planet 80 times more strongly than CO_2 over a 20-year period, even small changes have significant climate impacts. Its growth rate climbed to an unprecedented peak of 17.68±0.36 ppb/yr in 2021 before declining in subsequent years to 7.23±0.56 ppb/yr in 2024 (NOAA GML, https://gml.noaa.gov/ccgg/trends_ch4/). This abrupt sequence of extremes exposes fundamental gaps in our understanding of the atmospheric methane budget.

Methane is emitted from a diverse range of anthropogenic, biological, and geologic sources, many of which have large uncertainties, e.g., Kirschke et al., (2013); Lin et al., (2024); Saunois et al., (2025). The main loss of atmospheric methane is oxidation by the hydroxyl radical (OH). The resulting atmospheric chemistry lifetime of methane is approximately nine years. Because this loss term follows Arrhenius behaviour, even modest warming will increase reaction rates and reduce the global methane lifetime. It is because this lifetime is much shorter than CO_2, for example, that scientists and policymakers view reducing methane emissions as an effective short-term mitigation strategy (Folberth et al., 2024; Shindell et al., 2024).

Top-down Bayesian inversions, which integrate surface and satellite observations, provide quantitative constraints on methane emissions (e.g., Bergamaschi et al., (2013); Fraser et al., (2013); Lunt et al., (2019, 2021); Palmer et al., (2021); East et al., (2025)). However, their accuracy is fundamentally limited by uncertainties in the prescribed OH field, which is sensitive to changes in NOx (=NO+NO_2) emissions, ozone photochemistry, water vapour, temperature, and broader climate-driven shifts in atmospheric composition (Murray et al., 2014; Stevenson et al., 2022). As a result, changes in methane's atmospheric growth rate can plausibly arise from variability in either emissions or the sink, but current frameworks struggle to disentangle their contributions (Patra et al., 2011; Rigby et al., 2017; Qu et al., 2022; Jackson et al., 2024; Penn et al., 2025; Belikov et al., 2026).

This ambiguity has fuelled debate about the drivers of the rapid methane growth in 2020–2021. One explanation proposed a global reduction in the OH sink caused by pandemic-related declines in NOx emissions (e.g., Laughner et al., (2021); Peng et al., (2022); Stevenson et al., (2022); Ciais et al., (2026)). An alternative view, supported by satellite observations, identifies large and climate-sensitive emission anomalies in the tropics, particularly from wetlands, as major contributors to recent global trends (East et al., 2025; Feng et al., 2023; McNorton et al., 2022; Michel et al., 2024; Pendergrass et al., 2025; Qu et al.,

https://doi.org/10.5194/egusphere-2026-2662
Preprint. Discussion started: 29 May 2026

2022). These competing hypotheses highlight a central scientific challenge: the methane budget is simultaneously influenced by evolving natural emissions, anthropogenic activities, and chemically mediated changes in the atmospheric sink, yet existing observational constraints cannot cleanly partition their effects.

Here, we address this challenge using satellite retrievals from the Greenhouse Gases Observing Satellite (GOSAT) to jointly infer global and regional variations in methane emissions and OH concentrations from 2018 to 2024 By extending the framework developed in our previous work (Feng et al., 2023), we isolate the contributions of source and sink variability during this period of anomalous methane behaviour. Section 2 describes the observational datasets and inversion methodology; Section 3 presents the inferred global and regional budgets; and Section 4 discusses the implications for understanding recent methane trends and the sensitivity of the methane cycle to ongoing climate and chemical changes.

2 Data and Methods

We follow the methodology we use in a recent study (Feng et al., 2023) and for the sake of brevity only include details relevant to the calculation shown here.

2.1 GOSAT methane proxy data

We use version 9.0 of the proxy GOSAT XCH_4 retrievals from the University of Leicester, including both nadir observations over land and glint observations over the ocean. Analyses have shown that these retrievals have a bias of 0.2%, with a single-sounding precision of ~0.72% (Parker et al., 2020). We globally remove a slightly larger 0.3% bias from the GOSAT proxy XCH_4 retrievals to improve the comparison with independent in situ observations. We assume that each single GOSAT proxy XCH_4 retrieval has an uncertainty of 1.2% to account for possible model errors, including the errors in model CO_2 concentrations and errors in GEOS-Chem atmospheric chemistry and transport.

2.2 In situ data

We also ingest simultaneously methane mole fraction data collected at surface-based sites (Figure A1b) from the NOAA compilation of the multi-laboratory in situ measurements (Cox et al., 2021; Di Sarra et al., 2021, 2022; Cox et al., 2022; Schuldt et al., 2026). We use a similar subset of surface sites to those used in our previous studies (Feng et al., 2022) in which we examined, for example, year-to-year changes of methane emissions during 2010-2019. We assume uncertainties of 8 ppb for these in situ observations of methane (Feng et al., 2023). This assumed uncertainty is larger than typical instrument error, to account for model errors, particularly representation errors.

In this study, in situ observations provide anchor points and complementary constraints for the inversion experiments. Using different subsets of observations, for example, by including data from Integrated Carbon Observation System (ICOS) sites over western Europe ((ICOS RI et al., 2025) can affect regional flux estimates by up to several teragrams per year, but has

https://doi.org/10.5194/egusphere-2026-2662
Preprint. Discussion started: 29 May 2026

only a small impact on interannual variability in a posterior global methane emissions and sinks, remaining within the reported uncertainty range. This limited global influence reflects the use of inflated observation uncertainties and filtering that excludes observations deviating by more than three times the total uncertainty from short-term model forecasts, as well as the broad coverage provided by GOSAT proxy XCH_4 retrievals. Sensitivity tests further show that inversions using only GOSAT data reproduce the main results, including the relative contributions of emission and sink changes to the methane growth rate after 2019. Nevertheless, selected in situ observations improve agreement with independent datasets such as TCCON (Wunch et al., 2011), and support online bias correction of the GOSAT XCH_4 retrievals.

2.3 GEOS-Chem atmospheric chemistry transport model

We use the GEOS-Chem at a horizontal resolution of 2° (latitude) × 2.5° (longitude), driven by the MERRA2 meteorological reanalyses from the Global Modeling and Assimilation Office Global Circulation Model based at NASA Goddard Space Flight Center.

Our model calculations closely follow Feng et al., (2023). Our a priori natural methane fluxes include monthly wetland emissions, including rice paddies (Bloom et al., 2017); monthly fire methane emissions (van der Werf et al., 2017); and termite emissions (Fung et al., 1991). We include emissions from geological macroseeps (Kvenvolden and Rogers, 2005; Etiope, 2015). For a priori anthropogenic methane emissions we use the EDGAR v4.41 global emission inventory (Janssens-Maenhout et al., 2019) that includes various sources related to human activities (e.g., oil and gas industry, coal mining, livestock, and waste). We use monthly 3-D fields of OH as a priori, which consistent with observed values for the lifetime of methyl chloroform, from the GEOS-Chem full chemistry simulation (Mao et al., 2013; Turner et al., 2015) to describe the main oxidation sink of methane. Using pre-computed fields of OH greatly simplifies our calculations but they are unable to reflect any variations driven by short-term emission changes and long-term climate changes. So as described below, we also include the adjustment of OH fields into our joint assimilation of the ground-based and space-borne observations of atmospheric methane concentrations simultaneously.

2.4 Ensemble Kalman filter inverse method

We use an ensemble Kalman Filter (EnKF) framework to estimate simultaneously methane fluxes and OH field from satellite measurements of the atmospheric methane (Feng et al., 2023). Our state vector includes monthly scaling factors for 620 regional pulse-like basis functions (**Error! Reference source not found.**) that describe temporal and spatial patterns of methane fluxes. We define our land sub-regions by dividing the 11 TransCom–3 land regions (Gurney et al., 2004)) into 49 nearly equal-area sub-regions, with the exception for temperate Eurasia that has been divided into 130 sub-regions due to its large landmass. We use a 4-month moving lag window to reduce the computational costs for projecting the flux perturbation ensemble into observation space long after (>4 months) their emissions, beyond which time it is difficult to distinguish between the emitted signal from variations in the ambient background atmosphere (Fraser et al., 2014; Feng et al., 2017). Our a priori

https://doi.org/10.5194/egusphere-2026-2662
Preprint. Discussion started: 29 May 2026

fluxes are described above. For simplicity we assume a fixed uncertainty of 40% for coefficients corresponding to the a priori methane fluxes over each sub-region. We also assume that a priori errors for methane regional sources are correlated with a spatial correlation length of 300 km and with a temporal correlation of one month.

We include the monthly adjustment (or increasing) factors for OH fields over 6 latitude bands of width 25°, from -75° to 75° as part of state vector to be estimated together with monthly regional emissions by assimilating methane concentration observations. We adopt this configuration because the constraints on OH are derived from the methane decaying in the free troposphere, which is in turn only small part of observed XCH_4 variations, and preclude OH estimation at higher horizontal and vertical resolutions. In this study, we assume the a priori value of the six multiplicative adjustment factors to be zero, with a uniform uncertainty of 10%. This uncertainty is consistent with the range of interannual OH variability reported by recent studies (Morgenstern et al., 2025; Penn et al., 2025). Our sensitivity tests (not shown) indicate that using smaller or larger a priori uncertainties (±20%) has only minor impact (generally <3 Tg/yr) on the interannual variability of a posteriori global methane emissions and sinks, after the spin-up year (2018), which is the focus of this study.

We conduct a parallel inversion experiment using the same EnKF approach and same observation datasets, but with OH fields being fixed to the monthly climatology (i.e., the a priori). Hereafter we refer the joint OH-surface emission inversion, and the inversion with fixed OH climatology as Inv-OH and Clim-OH, respectively.

3 Results

We now examine how methane emissions and atmospheric oxidation have evolved over the period 2018–2024. Using the complementary Clim-OH and Inv-OH inversions, we quantify the extent to which interannual changes in OH, temperature-dependent reaction rates, and surface emissions shape the observed atmospheric methane record.

3.1 Changes in OH and the corresponding atmospheric methane loss

Figure 1a shows monthly OH adjustment factors corresponding to Inv-OH. The retrieved scaling factors for the mid- to high-latitude regions of both hemispheres show much larger relative variations than those in the low-latitude bands. In particular, the scaling factors over the mid-Southern Hemisphere band (25°S–50°S) show pronounced seasonal variability. This behaviour is likely driven by a combination of seasonal variations of satellite observation coverage and the reduced sensitivity of XCH_4 to scaling factors in these regions, due to the relatively low background OH concentrations. Such large variations also slow the numerical convergence of the optimization procedure. To manage computation time, we therefore use a fixed number of five iterations, which is sufficient for stabilizing both the regional flux estimates and the adjustment factors for the low-latitude bands. Figure 1b shows the resulting global mean OH column density. In 2020, OH declined by approximately 18%, reflecting the effects of COVID-19 lockdowns and broadly consistent with previous analyses (Peng et al., 2022; Stevenson et al., 2022;

https://doi.org/10.5194/egusphere-2026-2662
Preprint. Discussion started: 29 May 2026

Feng et al., 2023). Since then, we find that OH levels have largely recovered. Except for 2020, all estimated OH values between 2018 and 2024 lie between 1% and 15% above our a priori value.

Figure 2 shows the chemical OH loss of methane inferred from Inv-OH and from Clim-OH integrated over four large latitude bands: 90ºS-90ºN, 90ºS-30ºS, 30ºS-30ºN, and 30ºN-90ºN. For Clim-OH and Inv-OH, we find that the tropics (**Figure 2**c) account for about 60-70% of the global chemical sinks (**Figure 2**a), while the southern and northern extra tropics (**Figure 2**b,d) contribute less than 30-40% of the global values due to comparatively low atmospheric values of OH and methane. The Inv-OH experiment shows that global and regional OH sinks fluctuate from year to year, while the inversion using fixed OH climatology shows a steady increase. On a global scale, the Inv-OH methane loss due to OH is due mainly to changes from the northern extratropics (**Figure 2**d), with only a small change originating from the tropics since 2020 (**Figure 2**c). In contrast for Clim-OH, the year-to-year change in the methane loss is dominated by rapid increase over the tropics. Figure 3 shows the corresponding spatial distributions of methane loss due to OH oxidation, described as the difference between 2024 and 2019. When we use a monthly climatological OH field, we find a global a posteriori increases in methane sinks (Figure 3a), driven by the rise in a posteriori methane concentrations and the chemical reaction rates (as explained below). In contrast, when we allow for year-by-year OH changes (Figure 3b), we find that the methane sink increases moderately over the northern low latitudes (0–25°N), while decreasing across the other latitude bands.

For Clim-OH, even though our OH concentrations are not affected by the inversion, we do find year to year changes in methane loss because of the change in atmospheric methane and the change in the OH+methane reaction rate that is described as a temperature-dependent Arrhenius equation. We find that combined the methane loss increasing due to higher temperature and high methane number densities is about 31±6 Tg/yr, equivalent to a 5.6% increase between 2024 and 2019 from GEOS-Chem simulations forced by posterior emission estimates.

Using a 1-D model, we can attribute these year-to-year changes in the methane loss L to changes in the reaction rate k and mass M changes in OH and methane using this expression:

$$\frac{L_2^{CH4}}{L_1^{CH4}} = \frac{k_2^{OH+CH4}}{k_1^{OH+CH4}} \times \frac{M_2^{OH}}{M_1^{OH}} \times \frac{M_2^{CH4}}{M_1^{CH4}} \approx 1 + \left(\frac{k_2^{OH+CH4} - k_1^{OH+CH4}}{k_1^{OH+CH4}}\right) + \left(\frac{M_2^{OH} - M_1^{OH}}{M_1^{OH}}\right) + \left(\frac{M_2^{CH4} - M_1^{CH4}}{M_1^{CH4}}\right), \quad (1)$$

where the subscript denotes year 2019 and 2024, respectively. The r.h.s. expression is derived using $b/a = 1 + (b-a)/a$. When year to year changes in any of these three quantities is very small, we can ignore the corresponding bracketed expression. For example, when the mass of OH does not change between years, as with our Clim-OH inversion, the change of methane loss can be approximated by the sum of the percentage change in atmospheric methane and the percentage changes in the temperature-dependent reaction rate.

For Clim-OH, the OH mass change is zero, while the methane mass increases by 2.9%. Consequently, the reaction rate increases by 2.7%, corresponding to ~14 Tg/yr, which is significant, nearly the same amount of increase due to higher

https://doi.org/10.5194/egusphere-2026-2662
Preprint. Discussion started: 29 May 2026

atmospheric methane. This magnitude of change is consistent with the expected enhancement in OH oxidation associated with an atmospheric temperature increase of approximately 1.1 K. Due to the heterogeneous nature of the OH loss of methane (Fig. 3), Eq.1 can only be applied to Inv-OH on a global basis.

To isolate the temperature-driven component of the methane sink change, we compare methane loss across three forward GEOS-Chem simulations. The 2019 baseline uses a posteriori OH fields, a posteriori methane emissions for 2019, and the a posteriori methane initial condition at the start of 2019. Its 2024 counterpart uses the corresponding a posteriori OH, methane emissions, and initial concentrations for 2024.

In the first 2024 swapping experiment, we replace the a posteriori OH field, methane emissions, and initial methane concentrations with their 2019 values. The only remaining differences relative to the 2019 baseline are the 2024 meteorology (temperature and transport). The resulting 7.8 Tg/yr increase in methane sink is therefore attributed to the temperature increase between 2019 and 2024. A second 2024 swapping experiment, in which only the a posteriori emissions and initial methane concentrations are replaced with 2019 values, isolates the effect of the increasing atmospheric methane burden. This yields an estimated sink decrease of about 19.2 Tg/yr relative to the standard 2024 run. Finally, a third 2024 simulation in which only the a posteriori OH field is replaced with its 2019 counterpart produces a -23.2 Tg/yr change in sink, relative to the standard 2023 run, reflecting the impact of declining OH.

Combining these contributions gives a net 2019-20124 sink change of 3.8 Tg/yr (= 19.2 + 7.8 – 23.2), despite the substantial OH-driven sink reduction. This estimate is higher than the sink difference of -1 Tg/yr obtained directly from the two standard simulations, likely reflecting differences in methane transport between the swapping experiments and the baseline runs.

3.2 Changes in methane emissions

Figure 4 compares the a posteriori methane emission by Clim-OH and Inv-OH, aggregated over 4 latitude bands. Both inversions show a large global methane emission increase between 2019 and 2020. However, with OH being allowed to adjust, the emission increase in Inv-OH becomes ~63% percent lower than the Clim-OH with fixed OH field, 14 Tg/yr vs 37 Tg/yr. This result is largely consistent with previous study (Feng et al., 2023), but with larger reduction in emission increase (-23 Tg/yr vs -10 Tg/yr). We attribute the difference between the result reported here and that published by Feng et al, (2023) to the bias in proxy XCH_4 data as result of the possible bias in applied model XCO_2 data. Our previous work used directly the ratio without assuming a priori information about XCO_2, which showed an increase of ~27 Tg/yr even when we assumed for 2020 the climatological OH field. We find with our current inversion, our XCH_4 columns corresponding to our a posteriori methane emissions are up to 6 ppb higher than collocated TCCON observations at Park Fall USA (not shown). We find similar biases for some northern hemisphere sites. Such biases do not significantly affect the interannual variations of the inferred atmospheric methane growth rate.

https://doi.org/10.5194/egusphere-2026-2662
Preprint. Discussion started: 29 May 2026

We further assess the impacts of potential retrieval biases by implementing an on-line bias-correction scheme (Bergamaschi et al., 2013; Fraser et al., 2013). We assume that the monthly bias in the proxy GOSAT XCH_4 retrievals can be represented by a piecewise linear function with five evenly spaced latitude nodes at 60°S, 30°S, 0°, 30°N, and 60°N. The bias values at these nodes are estimated as part of the inversion, jointly constrained by satellite and in situ observations. We assume a zero a priori bias is assumed to zero with an uncertainty of 5 ppb. Figure A4 shows the inversion results. Compared with the control experiment (Inv-OH), the inversion with on-line bias correction (Inv-OH_BC; Figure A4c) suggests a substantially larger contribution from emission increases (~31±6 Tg/yr), compared to a much smaller contribution from sink reductions (~3.0 Tg/yr). Although Inv-OH_BC shows better global agreement with TCCON, we treat these results with caution due to potential interference between OH and bias estimates. To some extent, they represent a scenario that strongly favours the dominance of emission changes.

In 2024, the global emissions estimated by Clim-OH are about 31 Tg/yr higher than 2019, wheras Inv-OH shows only a small difference of about 1 Tg/yr between these two years. Over the tropics, both inversions show similar interannual variability with peak emissions in 2021, consistent with recent studies (Pendergrass et al., 2025; Ciais et al., 2026) and supported by our sensitivity analyses (Figures A3 and A4). However, we find significant differences over the southern and northern hemispheres. Figure 5 describes the spatial pattern of emission change between 2024 and 2019 for these two inversions, respectively. **Figure 6** shows substantial emission reduction over Tropical South America in 2024, which is further confirmed by Figure 7 that is discussed below. This reduction is likely to be caused by the extensive drought across the tropical South America in 2023 and 2024 (see Feng et al., (2025)), but further study is needed. Emissions from Tropical Asia also shows a decrease from a peak in 2021-2022 to 2023-2024 (Figure A2). In contrast, we find that North Africa shows a stable or slightly increased emissions, albeit with a large baseline value (Figure A2).

3.3 Changes in the global atmospheric growth rate of methane

We convert the net atmospheric methane mass increase (production minus loss) into an annual methane growth rate using a global scaling factor: a 2.78 Tg/year increase in global methane burden corresponds to 1 ppb/year rise in global methane mixing ratio. Figure 7a compared the a posteriori methane growth rates with NOAA observations. The two inversions reproduce the main feature of the interannual variation of the observed growth rates, such as peak values around 18.5 ppb/yr, shouldered by lower values in 2019 and 2024. Inv-OH is closer to values reported by NOAA with differences ranging from -1.0±2.1 ppb/yr (-12% % in 2019) to 2.5 ±2.1ppb/yr (+15% in 2020). Our growth rates are consistent with satellite observation and model simulation (Hachmeister et al., 2024). Figure 7b diagnoses the change of the Clim-OH atmospheric methane growth rate, relative to the 2019 value. When the OH field is fixed, the growth rate change is dominated by emission change. The increasing atmospheric methane loss rate is also due to larger atmospheric methane due to increased emissions and to faster reaction rate due to warmer temperatures. This acts as a growing but relatively small drag on the methane growth. Figure 7c shows the same analysis but for Inv-OH for which we infer a posteriori changes in OH and methane emissions. We find there

https://doi.org/10.5194/egusphere-2026-2662
Preprint. Discussion started: 29 May 2026

are substantial changes in OH throughout our study period, with a peak value in 2020, as previously reported, decreasing through to 2023 followed by a modest increase in 2024. This change in the loss of methane typically plays a small role in the a posteriori atmospheric methane growth rate estimate, except for 2020. For example, the ratio between the absolute growth-rate change driven by sinks and that driven by emissions is approximately 1.5 (6.1/4.0) in 2020, favouring changes in chemical loss, but rapidly declines to approximately 0.25 (2.5/10.2) by 2022, favouring changes in emissions. This pattern reflects the post-COVID recovery and stabilization of OH concentrations from 2020 to 2023, prior to the pronounced decrease observed in 2024 (Figure 1b). Our sensitivity studies (e.g., Figures A3) highlight the varying contributions of emissions and sinks in driving the global mean growth of atmospheric methane.

4. Concluding Remarks

We investigated the drivers of recent variability in atmospheric methane using an ensemble Kalman filter framework coupled to the GEOS-Chem chemical transport model. By jointly optimizing methane emissions and atmospheric OH concentrations for 2018–2024, we quantified how changes in surface sources and atmospheric oxidation have contributed to the observed evolution of atmospheric methane.

Our results highlight the critical importance of representing interannual variability in OH when interpreting methane trends. Allowing OH to adjust within the inversion substantially alters inferred emissions, particularly during 2019–2021. Although both the fixed-OH (Clim-OH) and variable-OH (Inv-OH) inversions reproduce the sharp increase in methane emissions between 2019 and 2020, the magnitude of the inferred increase is ~63% smaller in Inv-OH. Neglecting OH variability therefore leads to an exaggerated attribution of methane growth to emissions alone. At the same time, our analysis reinforces that changes in OH can mask—but not eliminate—the long-term upward pressure from anthropogenic and natural methane sources.

We also find that OH experienced a pronounced global decline in 2020, consistent with atmospheric disruptions associated with COVID-19 lockdowns but largely recovered thereafter. Interannual changes in OH exert only modest influence on the methane growth rate outside of 2020, yet they meaningfully reshape the inferred source-sink balance. This underscores that trend-attribution studies based on climatological OH fields risk conflating chemical and emission-driven contributions to methane growth.

A key finding is the significant sensitivity of the methane sink to warmer atmospheric temperatures. Through the Arrhenius-type response of the OH+methane reaction, we estimate that higher global temperatures and methane concentrations strengthened the methane loss rate by ~31±6 Tg/yr in 2024 under the climatological-OH configuration (~5.6%). The temperature-driven changes alone contribute nearly half of the extra methane sink (~14 Tg/yr) and will occur even when methane and OH concentrations remain constant, revealing that climate-driven acceleration of atmospheric chemistry is an increasingly important component of the methane mass balance. Nevertheless, variations in emissions remain the dominant driver of the methane growth rate in most years, especially outside 2020 when OH declined sharply.

https://doi.org/10.5194/egusphere-2026-2662
Preprint. Discussion started: 29 May 2026

A mass-balance perspective is essential for interpreting changes in atmospheric methane. Even when OH anomalies are large in relative terms, the absolute changes in global methane loss remain smaller than corresponding changes in methane emissions. This helps explain why the atmospheric methane burden continued to rise after 2020 despite the partial recovery of OH, and why regional emission anomalies, such as the substantial reductions over tropical South America during the 2023–2024 drought, remain clearly detectable.

Finally, our results emphasize the need for improved observational constraints on methane, particularly for satellite-derived XCH_4. Biases of several ppb can propagate through the inversion and materially affect inferred emissions. Although bias-correction schemes exist, their reliance on sparse validation data limits their robustness. Future work will therefore prioritize direct assimilation of XCH_4:XCO_2 proxy ratios, which avoids dependence on model XCO_2 fields and reduces systematic uncertainty, albeit with higher computational cost.

Overall, this study demonstrates that a balanced representation of both methane emissions and atmospheric chemistry is essential for understanding recent methane trends. Accurate attribution requires high-quality observations and a dynamic treatment of OH – without both, the true partitioning of methane sources and sinks cannot be reliably inferred.

Data availability

The University of Leicester GOSAT Proxy v9.0 XCH_4 data are available from the Centre for Environmental Data Analysis (CEDA) data repository at https://doi.org/10.5285/18ef8247f52a4cb6a14013f8235cc1eb. The in situ data are available from the CEDA and the Max Planck Institute for Biogeochemistry, Jena (MPI-BGC). Principal investigators include Martin Heimann (MPI-BGC), Elena Kozlova (CEDA), Reimo Leppert (MPI-BGC), Thomas Seifert (MPI-BGC), Helder Timas (INMG), Andrew Watson (CEDA), Justin Worsey (CEDA), Sönke Zaehle (MPI-BGC). The community-led GEOS-Chem model of atmospheric chemistry and model is maintained centrally by Harvard University (http://geos-chem.seas.harvard.edu), and is available on request. The ensemble Kalman filter code is publicly available as PyOSSE (https://www.nceo.ac.uk/data-tools/atmospheric-tools/).

Author contributions

LF and PIP designed the research; LF, PIP, and HW prepared the calculations; RJP and HB provided the GOSAT data and expert advice on its usage; EGN, SB, LC, EG, LH, EK, SMN, TR, RAFS, and MS provided atmospheric methane measurements from various in situ sites (e.g., CBW, CVO, KAS, JAR, SGP) and offered guidance on their usage. LF and PIP wrote the paper, with comments from the co-authors.

Competing interests

The contact author has declared that neither they nor their co-authors have any competing interests.

https://doi.org/10.5194/egusphere-2026-2662
Preprint. Discussion started: 29 May 2026

Acknowledgements

We thank the Japanese Aerospace Exploration Agency, National Institute for Environmental Studies, and the Ministry of Environment for the GOSAT data and their continued support as part of the Joint Research Agreements at the Universities of Edinburgh and Leicester. GOSAT retrievals were processed using the ALICE High-Performance Computing Facility at the University of Leicester. We thank all the scientists that submitted data to the methane Observation Package (ObsPack) data products, coordinated by NOAA ESRL, and making them freely available for scientific research. We gratefully acknowledge the Japan Meteorological Agency (JMA) for providing atmospheric methane observation data from Ryori (RYO), Minamitorishima (MNM), and Yonagunijima (YON). We thank Environment and Climate Change Canada for use of surface measurements from the Canadian network. We acknowledge ICOS PIs for providing methane data on various ICOS sites, including bir, cbw, cmn, hel, hbp, htm, hun, ipr, izo, jfj, jue, kit, kre, lin, lmp, lut, nor, ope, opw, oxk, pal, prs, pui, puy, rgl, run, sac, smr, stm, svb, toh, uto, vac, wes, zep, and zsf etc, for our inversion and sensitivity experiments. We also thank the GEOS-Chem community, particularly the team at Harvard University who help maintain the GEOS-Chem model, and the NASA Global Modeling and Assimilation Office (GMAO) who provide the MERRA2 data product.

Financial support:

L.F., P.I.P., and R.J.P. acknowledge support from the UK National Centre for Earth Observation funded by the National Environment Research Council (NE/R016518/1); R.J.P. also acknowledges funding from grant NE/N018079/1. We acknowledge funding from the Copernicus Climate Change Service (C3S2_312a_Lot2) related to generation of the GOSAT data.

References

Belikov, D.A., Patra, P.K., Saitoh, N., 2026. Hydroxyl Interannual Variability Impacts Estimation of Regional Methane Emissions. J. Geophys. Res. Atmospheres 131, e2025JD044457. https://doi.org/10.1029/2025JD044457

Bergamaschi, P., Houweling, S., Segers, A., Krol, M., Frankenberg, C., Scheepmaker, R.A., Dlugokencky, E., Wofsy, S.C., Kort, E.A., Sweeney, C., Schuck, T., Brenninkmeijer, C., Chen, H., Beck, V., Gerbig, C., 2013. Atmospheric CH4 in the first decade of the 21st century: Inverse modeling analysis using SCIAMACHY satellite retrievals and NOAA surface measurements. J. Geophys. Res. Atmospheres 118, 7350–7369. https://doi.org/10.1002/jgrd.50480

Bloom, A.A., Bowman, K.W., Lee, M., Turner, A.J., Schroeder, R., Worden, J.R., Weidner, R., McDonald, K.C., Jacob, D.J., 2017. A global wetland methane emissions and uncertainty dataset for atmospheric chemical transport models (WetCHARTs version 1.0). Geosci. Model Dev. 10, 2141–2156. https://doi.org/10.5194/gmd-10-2141-2017

Calvin, K., Dasgupta, D., Krinner, G., Mukherji, A., Thorne, P.W., Trisos, C., Romero, J., Aldunce, P., Barrett, K., Blanco, G., Cheung, W.W.L., Connors, S., Denton, F., Diongue-Niang, A., Dodman, D., Garschagen, M., Geden, O., Hayward, B., Jones, C., Jotzo, F., Krug, T., Lasco, R., Lee, Y.-Y., Masson-Delmotte, V., Meinshausen, M., Mintenbeck, K., Mokssit, A., Otto, F.E.L., Pathak, M., Pirani, A., Poloczanska, E., Pörtner, H.-O., Revi, A., Roberts, D.C., Roy, J., Ruane, A.C., Skea, J., Shukla, P.R., Slade, R., Slangen, A., Sokona, Y., Sörensson, A.A., Tignor, M., Van Vuuren, D., Wei, Y.-M., Winkler, H., Zhai, P., Zommers, Z., Hourcade, J.-C., Johnson, F.X., Pachauri, S., Simpson, N.P., Singh, C., Thomas, A., Totin, E., Alegría, A., Armour, K., Bednar-Friedl, B., Blok, K., Cissé, G., Dentener, F., Eriksen, S., Fischer, E., Garner, G., Guivarch, C., Haasnoot, M., Hansen, G., Hauser, M., Hawkins, E.,

https://doi.org/10.5194/egusphere-2026-2662
Preprint. Discussion started: 29 May 2026

Hermans, T., Kopp, R., Leprince-Ringuet, N., Lewis, J., Ley, D., Ludden, C., Niamir, L., Nicholls, Z., Some, S., Szopa, S., Trewin, B., Van Der Wijst, K.-I., Winter, G., Witting, M., Birt, A., Ha, M., 2023. IPCC, 2023: Climate Change 2023: Synthesis Report. Contribution of Working Groups I, II and III to the Sixth Assessment Report of the Intergovernmental Panel on Climate Change [Core Writing Team, H. Lee and J. Romero (eds.)]. IPCC, Geneva, Switzerland. Intergovernmental Panel on Climate Change (IPCC). https://doi.org/10.59327/IPCC/AR6-9789291691647

Ciais, P., Zhu, Y., Cai, Y., Lan, X., Michel, S.E., Zheng, B., Zhao, Y., Hauglustaine, D.A., Lin, X., Zhang, Y., Sun, S., Tian, X., Zhao, M., Wang, Y., Chang, J., Dou, X., Liu, Z., Andrew, R., Quinn, C.A., Poulter, B., Ouyang, Z., Yuan, W., Yuan, K., Zhu, Q., Li, F., Pan, N., Tian, H., Yu, X., Rocher-Ros, G., Johnson, M.S., Li, M., Li, M., Feng, D., Raymond, P., Yang, X., Canadell, J.G., Jackson, R.B., Yu, X., Li, Y., Saunois, M., Bousquet, P., Peng, S., 2026. Why methane surged in the atmosphere during the early 2020s. Science 391, eadx8262. https://doi.org/10.1126/science.adx8262

Cox, A., Di Sarra, A.G., Karion, A., Arlyn Andrews, Colomb, A., Scheeren, B., Paplawsky, B., Viner, B., Myhre, C.L., Miller, C.E., Plass-Duelmer, C., Plass-Duelmer, C., Sloop, C.D., Sweeney, C., Kubistin, D., Jaffe, D., Dlugokencky, E., Hintsa, E., Morgan, E., Vitkova, G., Manca, G., Huilin Chen, Lehner, I., Mammarella, I., Pichon, J.M., Müller-Williams, J., Miller, J.B., Lee, J., Hatakka, J., Holst, J., Kominkova, K., McKain, K., Thoning, K., Tørseth, K., Emmenegger, L., Merchant, L., Sha, M.K., Delmotte, M., Fischer, M.L., Schumacher, M., Leuenberger, M., Steinbacher, M., De Mazière, M., Lindauer, M., Mölder, M., Heliasz, M., Marek, M.V., Ramonet, M., Lopez, M., Laurent, O., Hermanssen, O., Trisolino, P., Cristofanelli, P., Smith, P., Bakwin, P., Bergamaschi, P., Keronen, P., Tans, P., Keeling, R., Piacentino, S., Biraud, S.C., Conil, S., Clark, S., De Wekker, S., Walker, S., Piper, S., Biermann, T., Laurila, T., Aalto, T., Kazan, V., 2022. Multi-laboratory compilation of atmospheric carbon dioxide data for the year 2021; obspack_co2_1_NRT_v7.1_2022-03-04. https://doi.org/10.25925/20220301

Cox, A., Di Sarra, A.G., Vermeulen, A., Manning, Alistair, Beyersdorf, A., Zahn, A., Manning, Andrew, Watson, A., Karion, A., Hensen, A., Arlyn Andrews, Frumau, A., Colomb, A., Scheeren, B., Law, B., Baier, B., Munger, B., Paplawsky, B., Viner, B., Stephens, B., Daube, B., Labuschagne, C., Myhre, C.L., Hanson, C., Miller, C.E., Plass-Duelmer, C., Plass-Duelmer, C., Gerbig, C., Sloop, C.D., Sweeney, C., Kubistin, D., Goto, D., Jaffe, D., Say, D., Van Dinther, D., Bowling, D., Lam, D.H.Y., Munro, D., Dickon Young, Worthy, D., Dlugokencky, E., Kozlova, E., Gloor, E., Cuevas, E., Reyes-Sanchez, E., Hintsa, E., Kort, E., Morgan, E., Obersteiner, F., Apadula, F., Francois Gheusi, Meinhardt, F., Moore, F., Vitkova, G., Chen, G., Bentz, G., Manca, G., Brailsford, G., Forster, G., Boenisch, H., Riris, H., Meijer, H., Timas, H., Matsueda, H., Huilin Chen, Levin, I., Lehner, I., Mammarella, I., Bartyzel, J., Abshire, J.B., Elkins, J.W., Levula, J., Jaroslaw Necki, Pichon, J.M., Peischl, J., Müller-Williams, J., Turnbull, J., Miller, J.B., Lee, J., Lin, J., Josep-Anton Morgui, DiGangi, J.P., Lavric, J., Hatakka, J., Coletta, J.D., Worsey, J., Holst, J., Kominkova, K., McKain, K., Saito, K., Aikin, K., Davis, K., Thoning, K., Tørseth, K., Haszpra, L., Mitchell, L., Gatti, L.V., Emmenegger, L., Lukasz Chmura, Merchant, L., Sha, M.K., Delmotte, M., Fischer, M.L., Schumacher, M., Torn, M., Leuenberger, M., Heimann, M., Steinbacher, M., De Mazière, M., Sargent, M., Lindauer, M., Mölder, M., Martin, M.Y., Shook, M., Galkowski, M., Heliasz, M., Marek, M.V., Ramonet, M., Miroslaw Zimnoch, Lopez, M., Sasakawa, M., N. Mihalopoulos, Miles, N., Lee, O.S.M., Laurent, O., Peltola, O., Hermanssen, O., Trisolino, P., Cristofanelli, P., Kolari, P., Krummel, P., Shepson, P., Smith, P., Rivas, P.P., Bakwin, P., Bergamaschi, P., Keronen, P., Tans, P., Van Den Bulk, P., Keeling, R., Ramos, R., Langenfelds, R., Leppert, R., Curcoll, R., Commane, R., Newman, S., Piacentino, S., Hammer, S., Richardson, S., Biraud, S.C., Conil, S., Clark, S., Morimoto, S., Shuangxi Fang, Aoki, S., O'Doherty, S., Sites Climadat, Zaehle, S., De Wekker, S., Kawa, S.R., Montzka, S., Walker, S., Piper, S., Wofsy, S., Nichol, S., Schuck, T., Lauvaux, T., Ryerson, T., Seifert, T., Griffis, T., Biermann, T., Gehrlein, T., Machida, T., Laurila, T., Aalto, T., Gomez-Trueba, V., Kazan, V., Ivakhov, V., Joubert, W., Niwa, Y., Loh, Z., 2021. Multi-laboratory compilation of atmospheric carbon dioxide data for the period 1957-2020; obspack_co2_1_GLOBALVIEWplus_v7.0_2021-08-18. https://doi.org/10.25925/20210801

Di Sarra, A.G., Ankur Desai, Karion, A., Arlyn Andrews, Colomb, A., Scheeren, B., Viner, B., Myhre, C.L., Couret, C., Miller, C.E., Plass-Duelmer, C., Plass-Duelmer, C., Sloop, C.D., Sweeney, C., Kubistin, D., Jaffe, D., Dlugokencky, E., Vitkova, G., Manca, G., Huilin Chen, Lehner, I., Mammarella, I., Pichon, J.M., Müller-Williams, J., Miller, J.B., Lee, J., Hatakka, J., Holst, J., Kominkova, K., McKain, K., Tørseth, K., Emmenegger, L., Sha, M.K., Delmotte, M., Fischer, M.L., Schumacher, M., Leuenberger, M., Steinbacher, M., Schmidt, M., De Mazière, M., Lindauer, M.,

https://doi.org/10.5194/egusphere-2026-2662
Preprint. Discussion started: 29 May 2026

Mölder, M., Heliasz, M., Marek, M.V., Ramonet, M., Lopez, M., Laurent, O., Hermanssen, O., Trisolino, P., Cristofanelli, P., Smith, P., Bergamaschi, P., Keronen, P., Piacentino, S., Biraud, S.C., Conil, S., Biermann, T., Laurila, T., Aalto, T., Kazan, V., 2022. Multi-laboratory compilation of atmospheric methane data for the year 2021; obspack_ch4_1_NRT_v4.0_2022-03-03. https://doi.org/10.25925/20211101

Di Sarra, A.G., Zahn, A., Watson, A., Ankur Desai, Karion, A., Arlyn Andrews, Colomb, A., Scheeren, B., Baier, B., Viner, B., Stephens, B., Daube, B., Labuschagne, C., Myhre, C.L., Miller, C.E., Choong-Hoon Lee, Plass-Duelmer, C., Plass-Duelmer, C., Gerbig, C., Sloop, C.D., Sweeney, C., Kubistin, D., Goto, D., Jaffe, D., Munro, D., Worthy, D., Dlugokencky, E., Kozlova, E., Gloor, E., Cuevas, E., Hintsa, E., Kort, E., Obersteiner, F., Moore, F., Vitkova, G., Manca, G., Brailsford, G., Santoni, G., Haeyoung Lee, Boenisch, H., Timas, H., Matsueda, H., Kang, H.-Y., Huilin Chen, Lehner, I., Mammarella, I., Elkins, J.W., Pittman, J., Pichon, J.M., Müller-Williams, J., Jgor Arduini, Turnbull, J., Miller, J.B., Lee, J., DiGangi, J.P., Hatakka, J., Worsey, J., Holst, J., Kominkova, K., McKain, K., Saito, K., Davis, K., Tørseth, K., Haszpra, L., Gatti, L.V., Emmenegger, L., Sha, M.K., Delmotte, M., Fischer, M.L., Schumacher, M., Torn, M., Leuenberger, M., Heimann, M., Steinbacher, M., De Mazière, M., Lindauer, M., Mölder, M., Martin, M.Y., Ko, M.-Y., Heliasz, M., Marek, M.V., Ramonet, M., Lopez, M., Sasakawa, M., Miles, N., Laurent, O., Hermanssen, O., Trisolino, P., Cristofanelli, P., Krummel, P., Shepson, P., Smith, P., Rivas, P.P., Bergamaschi, P., Keronen, P., Langenfelds, R., Leppert, R., Piacentino, S., Richardson, S., Biraud, S.C., Conil, S., Morimoto, S., Aoki, S., O'Doherty, S., Wofsy, S., Nichol, S., Schuck, T., Lauvaux, T., Seifert, T., Biermann, T., Gehrlein, T., Machida, T., Laurila, T., Aalto, T., Kazan, V., Ivakhov, V., Joubert, W., Niwa, Y., Loh, Z., 2021. Multi-laboratory compilation of atmospheric methane data for the period 1983-2020; obspack_ch4_1_GLOBALVIEWplus_v4.0_2021-10-14. https://doi.org/10.25925/20211001

East, J.D., Jacob, D.J., Jervis, D., Balasus, N., Estrada, L.A., Hancock, S.E., Sulprizio, M.P., Thomas, J., Wang, X., Chen, Z., Varon, D.J., Worden, J.R., 2025. Worldwide inference of national methane emissions by inversion of satellite observations with UNFCCC prior estimates. Nat. Commun. 16, 11004. https://doi.org/10.1038/s41467-025-67122-8

Etiope, E., 2015. Natural Gas Seepage: The Earth's Hydrocarbon Degassing. Springer.

Feng, L., Palmer, P.I., Bösch, H., Parker, R.J., Webb, A.J., Correia, C.S.C., Deutscher, N.M., Domingues, L.G., Feist, D.G., Gatti, L.V., Others, 2017. Consistent regional fluxes of CH_4 and CO_2 inferred from GOSAT proxy XCH_4: XCO_2 retrievals, 2010--2014. Atmos Chem Phys 17, 4781–4797.

Feng, L., Palmer, P.I., Parker, R.J., Lunt, M.F., Bösch, H., 2023. Methane emissions are predominantly responsible for record-breaking atmospheric methane growth rates in 2020 and 2021. Atmospheric Chem. Phys. 23, 4863–4880. https://doi.org/10.5194/acp-23-4863-2023

Feng, L., Palmer, P.I., Smallman, L., Xiao, J., Cristofanelli, P., Hermansen, O., Lee, J., Labuschagne, C., Montaguti, S., Noe, S.M., Platt, S.M., Ren, X., Steinbacher, M., Xueref-Remy, I., 2025. The role of the tropical carbon balance in determining the large atmospheric CO_2 growth rate in 2023. Atmospheric Chem. Phys. 25, 13053–13076. https://doi.org/10.5194/acp-25-13053-2025

Feng, L., Palmer, P.I., Zhu, S., Parker, R.J., Liu, Y., 2022. Tropical methane emissions explain large fraction of recent changes in global atmospheric methane growth rate. Nat. Commun. 13, 1378. https://doi.org/10.1038/s41467-022-28989-z

Folberth, G., O'Connor, F., Jones, C., Gedney, N., Wiltshire, A., 2024. Drivers of persistent changes in the global methane cycle under aggressive mitigation action. https://doi.org/10.21203/rs.3.rs-4078060/v1

Fraser, A., Palmer, P.I., Feng, L., Boesch, H., Cogan, A., Parker, R., Dlugokencky, E.J., Fraser, P.J., Krummel, P.B., Langenfelds, R.L., O'Doherty, S., Prinn, R.G., Steele, L.P., van der Schoot, M., Weiss, R.F., 2013. Estimating regional methane surface fluxes: the relative importance of surface and GOSAT mole fraction measurements. Atmospheric Chem. Phys. 13, 5697–5713. https://doi.org/10.5194/acp-13-5697-2013

Fraser, A., Palmer, P.I., Feng, L., Bösch, H., Parker, R., Dlugokencky, E.J., Krummel, P.B., Langenfelds, R.L., 2014. Estimating regional fluxes of CO_2 and CH_4 using space-borne observations of XCH_4: XCO_2. Atmospheric Chem. Phys. 14. https://doi.org/10.5194/acp-14-12883-2014

Fung, I., John, J., Lerner, J., Matthews, E., Prather, M., Steele, L.P., Fraser, P.J., 1991. Three-dimensional model synthesis of the global methane cycle. J. Geophys. Res. Atmospheres 96, 13033–13065. https://doi.org/10.1029/91JD01247

Gurney, K.R., Law, R.M., Denning, A.S., Rayner, P.J., Pak, B.C., Baker, D., Bousquet, P., Bruhwiler, L., Chen, Y.-H., Ciais, P., Fung, I.Y., Heimann, M., John, J., Maki, T., Maksyutov, S., Peylin, P., Prather, M., Taguchi, S., 2004. Transcom

https://doi.org/10.5194/egusphere-2026-2662
Preprint. Discussion started: 29 May 2026

3 inversion intercomparison: Model mean results for the estimation of seasonal carbon sources and sinks. Glob. Biogeochem. Cycles 18. https://doi.org/10.1029/2003GB002111

Hachmeister, J., Schneising, O., Buchwitz, M., Burrows, J.P., Notholt, J., Buschmann, M., 2024. Zonal variability of methane trends derived from satellite data. Atmospheric Chem. Phys. 24, 577–595. https://doi.org/10.5194/acp-24-577-2024

ICOS RI, Apadula, F., Arnold, S., Bergamaschi, P., Biermann, T., Chen, H., Colomb, A., Conil, S., Couret, C., Cristofanelli, P., De Mazière, M., Delmotte, M., Di Iorio, T., Emmenegger, L., Forster, G., Frumau, A., Harris, E., Haszpra, L., Hatakka, J., Heliasz, M., Heltai, D., Hensen, A., Hermansen, O., Hoheisel, A., Kneuer, T., Komínková, K., Kubistin, D., Larmanou, E., Laurent, O., Laurila, T., Lehner, I., Lehtinen, K., Leskinen, A., Leuenberger, M., Levula, J., Lindauer, M., Lopez, M., Lund Myhre, C., Lunder, C., Mammarella, I., Manca, G., Manning, A., Marek, M.V., Marklund, P., Meinhardt, F., Miettinen, P., Molnár, M., Montaguti, S., Mölder, M., Müller-Williams, J., O'Doherty, S., Ottosson-Löfvenius, M., Piacentino, S., Pichon, J.-M., Pitt, J., Platt, S.M., Plaß-Dülmer, C., Ramonet, M., Rivas-Soriano, P., Roulet, Y.-A., Scheeren, B., Schmidt, M., Schumacher, M., Sferlazzo, D., Sha, M.K., Smith, P., Stanley, K., Steinbacher, M., Sørensen, L.L., Trisolino, P., Vítková, G., Ylisirniö, A., Yver-Kwok, C., Zazzeri, G., Zwerschke, E., di Sarra, A., ICOS ATC-Laboratoires des Sciences du Climat et de L'Environnement (LSCE), France, ICOS Central Radiocarbon Laboratory (CRL), Germany, ICOS Flask And Calibration Laboratory (FCL), Germany, ICOS-CAL-CRL, ICOS-CAL-FCL, 2025. ICOS Atmosphere Release 2025-1 of Level 2 Greenhouse Gas Mole Fractions of CO2, CH4, N2O, CO, meteorology and 14CO2, and flask samples analysed for CO2, CH4, N2O, CO, H2, SF6, delta 13C CO2, delta18OCO2, delta O2N2 and 14C. https://doi.org/10.18160/PP29-9CNZ

Jackson, R.B., Saunois, M., Martinez, A., Canadell, J.G., Yu, X., Li, M., Poulter, B., Raymond, P.A., Regnier, P., Ciais, P., Davis, S.J., Patra, P.K., 2024. Human activities now fuel two-thirds of global methane emissions. Environ. Res. Lett. 19, 101002. https://doi.org/10.1088/1748-9326/ad6463

Janssens-Maenhout, G., Crippa, M., Guizzardi, D., Muntean, M., Schaaf, E., Dentener, F., Bergamaschi, P., Pagliari, V., Olivier, J.G.J., Peters, J.A.H.W., van Aardenne, J.A., Monni, S., Doering, U., Petrescu, A.M.R., Solazzo, E., Oreggioni, G.D., 2019. EDGAR v4.3.2 Global Atlas of the three major greenhouse gas emissions for the period 1970--2012. Earth Syst. Sci. Data 11, 959–1002. https://doi.org/10.5194/essd-11-959-2019

Kirschke, S., Bousquet, P., Ciais, P., Saunois, M., Canadell, J.G., Dlugokencky, E.J., Bergamaschi, P., Bergmann, D., Blake, D.R., Bruhwiler, L., Cameron-Smith, P., Castaldi, S., Chevallier, F., Feng, L., Fraser, A., Heimann, M., Hodson, E.L., Houweling, S., Josse, B., Fraser, P.J., Krummel, P.B., Lamarque, J.-F., Langenfelds, R.L., Le Quéré, C., Naik, V., O'Doherty, S., Palmer, P.I., Pison, I., Plummer, D., Poulter, B., Prinn, R.G., Rigby, M., Ringeval, B., Santini, M., Schmidt, M., Shindell, D.T., Simpson, I.J., Spahni, R., Steele, L.P., Strode, S.A., Sudo, K., Szopa, S., van der Werf, G.R., Voulgarakis, A., van Weele, M., Weiss, R.F., Williams, J.E., Zeng, G., 2013. Three decades of global methane sources and sinks. Nat. Geosci. 6, 813–823. https://doi.org/10.1038/ngeo1955

Kvenvolden, K.A., Rogers, B.W., 2005. Gaia's breath's global methane exhalations. Mar. Pet. Geol. 22, 579–590. https://doi.org/10.1016/j.marpetgeo.2004.08.004

Lan, X., Thoning, K.W., Dlugokencky, E.J., 2026. Carbon Cycle Greenhouse Gases - NOAA Global Monitoring Laboratory [WWW Document]. URL https://gml.noaa.gov/ccgg/trends_doi.html (accessed 5.7.26).

Laughner, J.L., Neu, J.L., Schimel, D., Wennberg, P.O., Barsanti, K., Bowman, K.W., Chatterjee, A., Croes, B.E., Fitzmaurice, H.L., Henze, D.K., Kim, J., Kort, E.A., Liu, Z., Miyazaki, K., Turner, A.J., Anenberg, S., Avise, J., Cao, H., Crisp, D., de Gouw, J., Eldering, A., Fyfe, J.C., Goldberg, D.L., Gurney, K.R., Hasheminassab, S., Hopkins, F., Ivey, C.E., Jones, D.B.A., Liu, J., Lovenduski, N.S., Martin, R.V., McKinley, G.A., Ott, L., Poulter, B., Ru, M., Sander, S.P., Swart, N., Yung, Y.L., Zeng, Z.-C., 2021. Societal shifts due to COVID-19 reveal large-scale complexities and feedbacks between atmospheric chemistry and climate change. Proc. Natl. Acad. Sci. 118, e2109481118. https://doi.org/10.1073/pnas.2109481118

Lin, X., Peng, S., Ciais, P., Hauglustaine, D., Lan, X., Liu, G., Ramonet, M., Xi, Y., Yin, Y., Zhang, Z., Bösch, H., Bousquet, P., Chevallier, F., Dong, B., Gerlein-Safdi, C., Halder, S., Parker, R.J., Poulter, B., Pu, T., Remaud, M., Runge, A., Saunois, M., Thompson, R.L., Yoshida, Y., Zheng, B., 2024. Recent methane surges reveal heightened emissions from tropical inundated areas. Nat. Commun. 15, 10894. https://doi.org/10.1038/s41467-024-55266-y

Loulergue, L., Schilt, A., Spahni, R., Masson-Delmotte, V., Blunier, T., Lemieux, B., Barnola, J.-M., Raynaud, D., Stocker, T.F., Chappellaz, J., 2008. Orbital and millennial-scale features of atmospheric CH4 over the past 800,000 years. Nature 453, 383–386. https://doi.org/10.1038/nature06950

https://doi.org/10.5194/egusphere-2026-2662
Preprint. Discussion started: 29 May 2026

Lunt, M.F., Palmer, P.I., Feng, L., Taylor, C.M., Boesch, H., Parker, R.J., 2019. An increase in methane emissions from tropical Africa between 2010 and 2016 inferred from satellite data. Atmospheric Chem. Phys. 19, 14721–14740. https://doi.org/10.5194/acp-19-14721-2019

Lunt, M.F., Palmer, P.I., Lorente, A., Borsdorff, T., Landgraf, J., Parker, R.J., Boesch, H., 2021. Rain-fed pulses of methane from East Africa during 2018–2019 contributed to atmospheric growth rate. Environ. Res. Lett. 16, 024021. https://doi.org/10.1088/1748-9326/abd8fa

Mao, J., Paulot, F., Jacob, D.J., Cohen, R.C., Crounse, J.D., Wennberg, P.O., Keller, C.A., Hudman, R.C., Barkley, M.P., Horowitz, L.W., 2013. Ozone and organic nitrates over the eastern United States: Sensitivity to isoprene chemistry. J. Geophys. Res. Atmospheres 118, 11,211-256,268. https://doi.org/10.1002/jgrd.50817

McNorton, J., Bousserez, N., Agustí-Panareda, A., Balsamo, G., Cantarello, L., Engelen, R., Huijnen, V., Inness, A., Kipling, Z., Parrington, M., Ribas, R., 2022. Quantification of methane emissions from hotspots and during COVID-19 using a global atmospheric inversion. Atmospheric Chem. Phys. 22, 5961–5981. https://doi.org/10.5194/acp-22-5961-2022

Michel, S.E., Lan, X., Miller, J., Tans, P., Clark, J.R., Schaefer, H., Sperlich, P., Brailsford, G., Morimoto, S., Moossen, H., Li, J., 2024. Rapid shift in methane carbon isotopes suggests microbial emissions drove record high atmospheric methane growth in 2020-2022. Proc. Natl. Acad. Sci. U. S. A. 121, e2411212121. https://doi.org/10.1073/pnas.2411212121

Morgenstern, O., Moss, R., Manning, M., Zeng, G., Schaefer, H., Usoskin, I., Turnbull, J., Brailsford, G., Nichol, S., Bromley, T., 2025. Radiocarbon monoxide indicates increasing atmospheric oxidizing capacity. Nat. Commun. 16, 249. https://doi.org/10.1038/s41467-024-55603-1

Murray, L.T., Mickley, L.J., Kaplan, J.O., Sofen, E.D., Pfeiffer, M., Alexander, B., 2014. Factors controlling variability in the oxidative capacity of the troposphere since the Last Glacial Maximum. Atmospheric Chem. Phys. 14, 3589–3622. https://doi.org/10.5194/acp-14-3589-2014

Palmer, P.I., Feng, L., Lunt, M.F., Parker, R.J., Bösch, H., Lan, X., Lorente, A., Borsdorff, T., 2021. The added value of satellite observations of methane forunderstanding the contemporary methane budget. Philos. Trans. R. Soc. Math. Phys. Eng. Sci. 379, 20210106. https://doi.org/10.1098/rsta.2021.0106

Parker, R.J., Webb, A., Boesch, H., Somkuti, P., Barrio Guillo, R., Di Noia, A., Kalaitzi, N., Anand, J.S., Bergamaschi, P., Chevallier, F., Palmer, P.I., Feng, L., Deutscher, N.M., Feist, D.G., Griffith, D.W.T., Hase, F., Kivi, R., Morino, I., Notholt, J., Oh, Y.-S., Ohyama, H., Petri, C., Pollard, D.F., Roehl, C., Sha, M.K., Shiomi, K., Strong, K., Sussmann, R., Té, Y., Velazco, V.A., Warneke, T., Wennberg, P.O., Wunch, D., 2020. A decade of GOSAT Proxy satellite CH_4 observations. Earth Syst. Sci. Data 12, 3383–3412. https://doi.org/10.5194/essd-12-3383-2020

Patra, P.K., Houweling, S., Krol, M., Bousquet, P., Belikov, D., Bergmann, D., Bian, H., Cameron-Smith, P., Chipperfield, M.P., Corbin, K., Fortems-Cheiney, A., Fraser, A., Gloor, E., Hess, P., Ito, A., Kawa, S.R., Law, R.M., Loh, Z., Maksyutov, S., Meng, L., Palmer, P.I., Prinn, R.G., Rigby, M., Saito, R., Wilson, C., 2011. TransCom model simulations of CH_4 and related species: linking transport, surface flux and chemical loss with CH_4 variability in the troposphere and lower stratosphere. Atmospheric Chem. Phys. 11, 12813–12837. https://doi.org/10.5194/acp-11-12813-2011

Pendergrass, D.C., Jacob, D.J., Balasus, N., Estrada, L., Varon, D.J., East, J.D., He, M., Mooring, T.A., Penn, E., Nesser, H., Worden, J.R., 2025. Trends and seasonality of 2019–2023 global methane emissions inferred from a localized ensemble transform Kalman filter (CHEEREIO v1.3.1) applied to TROPOMI satellite observations. Atmospheric Chem. Phys. 25, 14353–14369. https://doi.org/10.5194/acp-25-14353-2025

Peng, S., Lin, X., Thompson, R.L., Xi, Y., Liu, G., Hauglustaine, D., Lan, X., Poulter, B., Ramonet, M., Saunois, M., Yin, Y., Zhang, Z., Zheng, B., Ciais, P., 2022. Wetland emission and atmospheric sink changes explain methane growth in 2020. Nature 612, 477–482. https://doi.org/10.1038/s41586-022-05447-w

Penn, E., Jacob, D.J., Chen, Z., East, J.D., Sulprizio, M.P., Bruhwiler, L., Maasakkers, J.D., Nesser, H., Qu, Z., Zhang, Y., Worden, J., 2025. What can we learn about tropospheric OH from satellite observations of methane? Atmospheric Chem. Phys. 25, 2947–2965. https://doi.org/10.5194/acp-25-2947-2025

Qu, Z., Jacob, D.J., Zhang, Y., Shen, L., Varon, D.J., Lu, X., Scarpelli, T., Bloom, A., Worden, J., Parker, R.J., 2022. Attribution of the 2020 surge in atmospheric methane by inverse analysis of GOSAT observations. Environ. Res. Lett. 17, 094003. https://doi.org/10.1088/1748-9326/ac8754

https://doi.org/10.5194/egusphere-2026-2662
Preprint. Discussion started: 29 May 2026

Rigby, M., Montzka, S.A., Prinn, R.G., White, J.W.C., Young, D., O'Doherty, S., Lunt, M.F., Ganesan, A.L., Manning, A.J., Simmonds, P.G., Salameh, P.K., Harth, C.M., Mühle, J., Weiss, R.F., Fraser, P.J., Steele, L.P., Krummel, P.B., McCulloch, A., Park, S., 2017. Role of atmospheric oxidation in recent methane growth. Proc. Natl. Acad. Sci. 114, 5373–5377. https://doi.org/10.1073/pnas.1616426114

Saunois, M., Martinez, A., Poulter, B., Zhang, Z., Raymond, P.A., Regnier, P., Canadell, J.G., Jackson, R.B., Patra, P.K., Bousquet, P., Ciais, P., Dlugokencky, E.J., Lan, X., Allen, G.H., Bastviken, D., Beerling, D.J., Belikov, D.A., Blake, D.R., Castaldi, S., Crippa, M., Deemer, B.R., Dennison, F., Etiope, G., Gedney, N., Höglund-Isaksson, L., Holgerson, M.A., Hopcroft, P.O., Hugelius, G., Ito, A., Jain, A.K., Janardanan, R., Johnson, M.S., Kleinen, T., Krummel, P.B., Lauerwald, R., Li, T., Liu, X., McDonald, K.C., Melton, J.R., Mühle, J., Müller, J., Murguia-Flores, F., Niwa, Y., Noce, S., Pan, S., Parker, R.J., Peng, C., Ramonet, M., Riley, W.J., Rocher-Ros, G., Rosentreter, J.A., Sasakawa, M., Segers, A., Smith, S.J., Stanley, E.H., Thanwerdas, J., Tian, H., Tsuruta, A., Tubiello, F.N., Weber, T.S., van der Werf, G.R., Worthy, D.E.J., Xi, Y., Yoshida, Y., Zhang, W., Zheng, B., Zhu, Qing, Zhu, Qiuan, Zhuang, Q., 2025. Global Methane Budget 2000–2020. Earth Syst. Sci. Data 17, 1873–1958. https://doi.org/10.5194/essd-17-1873-2025

Schuldt, K.N., Aalto, T., Aaltonen, H., Marcos Andrade, 2026. Multi-laboratory compilation of atmospheric carbon dioxide data for the period 1983-2024; obspack_ch4_1_GLOBALVIEWplus_v8.0_2026-01-13 [WWW Document]. URL https://commons.datacite.org/doi.org/10.25925/20251001 (accessed 5.8.26).

Shindell, D., Sadavarte, P., Aben, I., Bredariol, T. de O., Dreyfus, G., Höglund-Isaksson, L., Poulter, B., Saunois, M., Schmidt, G.A., Szopa, S., Rentz, K., Parsons, L., Qu, Z., Faluvegi, G., Maasakkers, J.D., 2024. The methane imperative. Front. Sci. 2. https://doi.org/10.3389/fsci.2024.1349770

Stevenson, D.S., Derwent, R.G., Wild, O., Collins, W.J., 2022. COVID-19 lockdown emission reductions have the potential to explain over half of the coincident increase in global atmospheric methane. Atmospheric Chem. Phys. 22, 14243–14252. https://doi.org/10.5194/acp-22-14243-2022

Turner, A.J., Jacob, D.J., Wecht, K.J., Maasakkers, J.D., Lundgren, E., Andrews, A.E., Biraud, S.C., Boesch, H., Bowman, K.W., Deutscher, N.M., Dubey, M.K., Griffith, D.W.T., Hase, F., Kuze, A., Notholt, J., Ohyama, H., Parker, R., Payne, V.H., Sussmann, R., Sweeney, C., Velazco, V.A., Warneke, T., Wennberg, P.O., Wunch, D., 2015. Estimating global and North American methane emissions with high spatial resolution using GOSAT satellite data. Atmospheric Chem. Phys. 15, 7049–7069. https://doi.org/10.5194/acp-15-7049-2015

van der Werf, G.R., Randerson, J.T., Giglio, L., van Leeuwen, T.T., Chen, Y., Rogers, B.M., Mu, M., van Marle, M.J.E., Morton, D.C., Collatz, G.J., Yokelson, R.J., Kasibhatla, P.S., 2017. Global fire emissions estimates during 1997--2016. Earth Syst. Sci. Data 9, 697–720. https://doi.org/10.5194/essd-9-697-2017

WMO, 2025. WMO Greenhouse Gas Bulletin - No. 21 [WWW Document]. World Meteorol. Organ. URL https://wmo.int/resources/publication-series/greenhouse-gas-bulletin/wmo-greenhouse-gas-bulletin-no-21 (accessed 5.8.26).

Wunch, D., Toon, G.C., Blavier, J.-F.L., Washenfelder, R.A., Notholt, J., Connor, B.J., Griffith, D.W.T., Sherlock, V., Wennberg, P.O., 2011. The Total Carbon Column Observing Network. Philos. Trans. R. Soc. Math. Phys. Eng. Sci. 369, 2087–2112. https://doi.org/10.1098/rsta.2010.0240

https://doi.org/10.5194/egusphere-2026-2662
Preprint. Discussion started: 29 May 2026

Figures

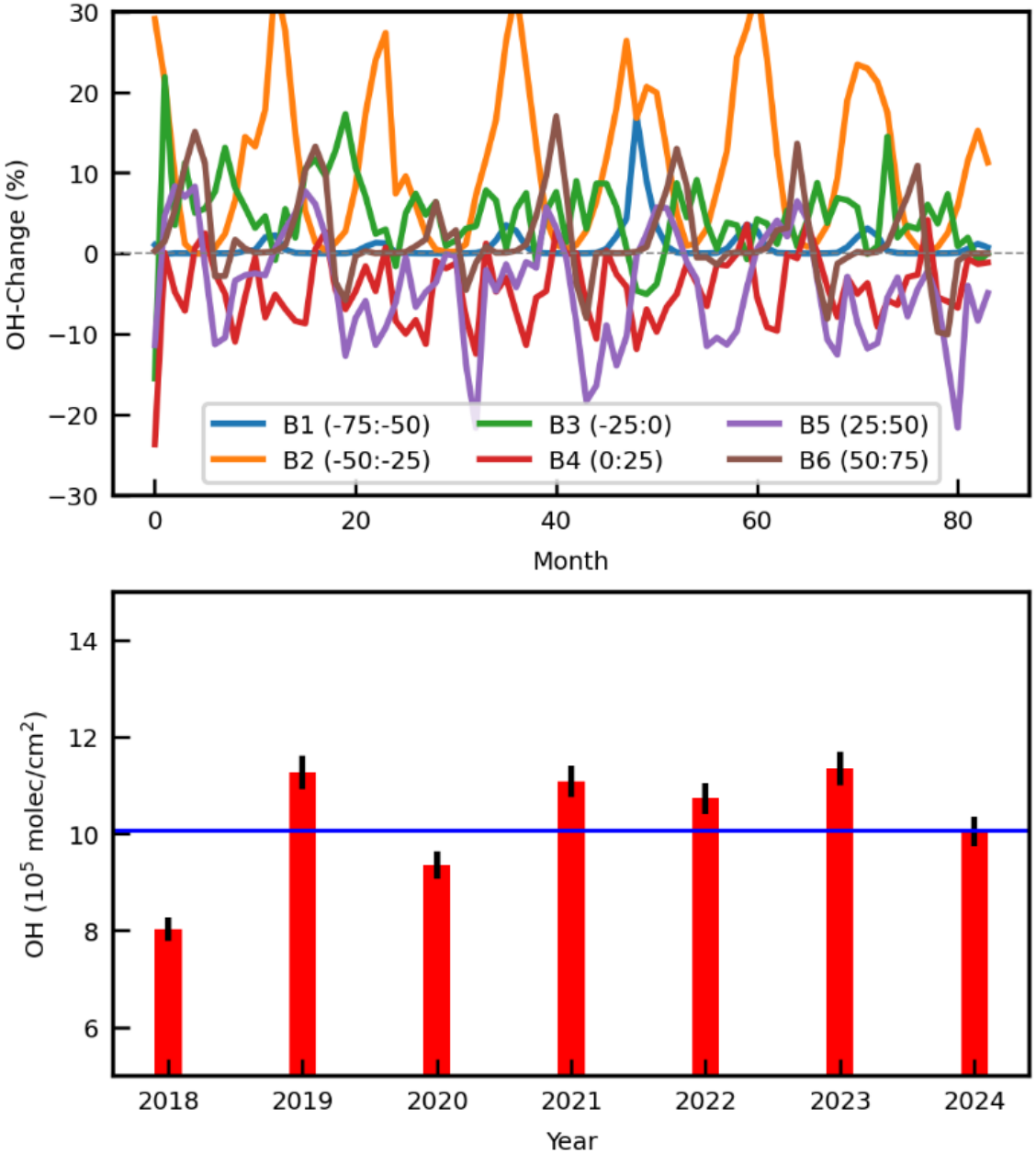

Figure 1: (**a**) Top panel show the a posteriori OH adjustment factor (positive means increase) for 6 bands with an uniform width of 25° spanning from -75° to 75°. (**b**) Lower panel shows a posteriori global mean OH column density. The dashed line in panel a denotes zero change line, and the blue line in panel b denotes the climatological a priori value for OH.

https://doi.org/10.5194/egusphere-2026-2662
Preprint. Discussion started: 29 May 2026

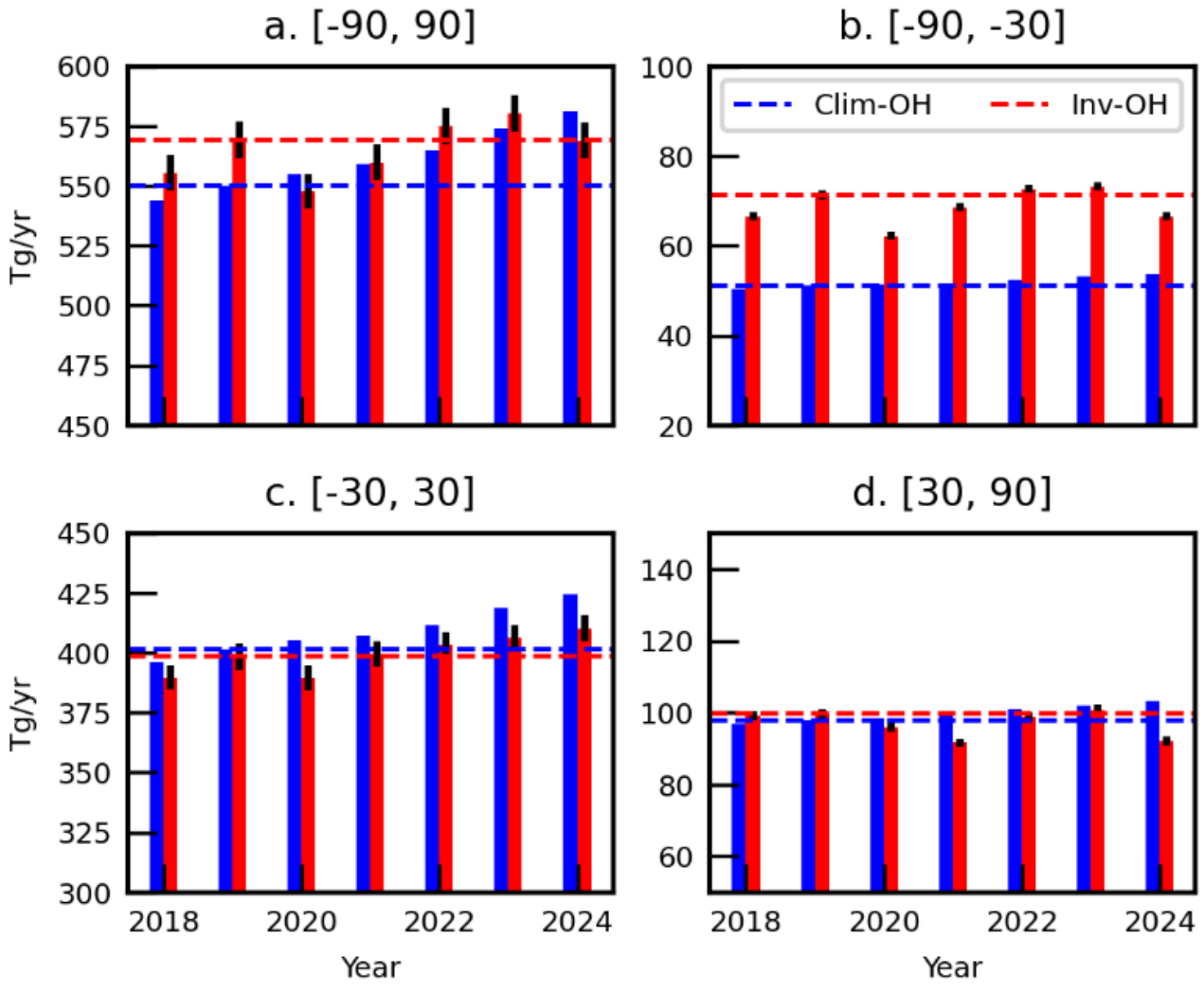

Figure 2: Annual mean values for the chemical loss of methane, 2018-2024, due to oxidation by OH for Clim-OH (blue) and Inv-OH (red) inversions. Panels show results for the (**a**) globe, (**b**) southern extratropics, (**c**) tropics, and (**d**) northern extratropics. The blue and red horizontal dashed lines denote a priori values for the Clim-OH and Inv-OH inversions in 2019, respectively.

https://doi.org/10.5194/egusphere-2026-2662
Preprint. Discussion started: 29 May 2026

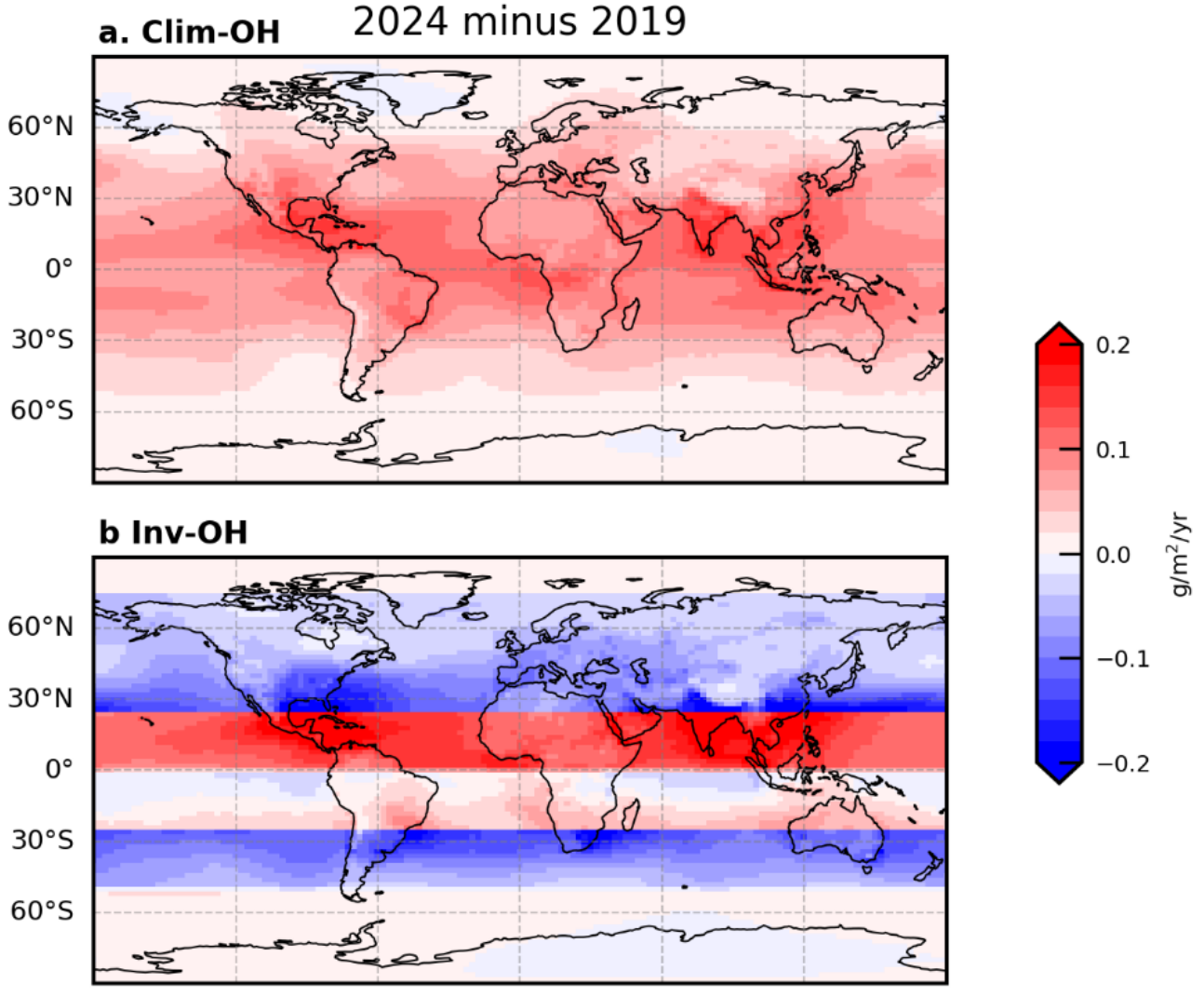

600 **Figure 3**: Annual mean spatial distribution of the difference in methane loss due to oxidation by OH, 2024 minus 2019 for (**a**) Clim-OH; and (**b**) Inv-OH inversions.

https://doi.org/10.5194/egusphere-2026-2662
Preprint. Discussion started: 29 May 2026

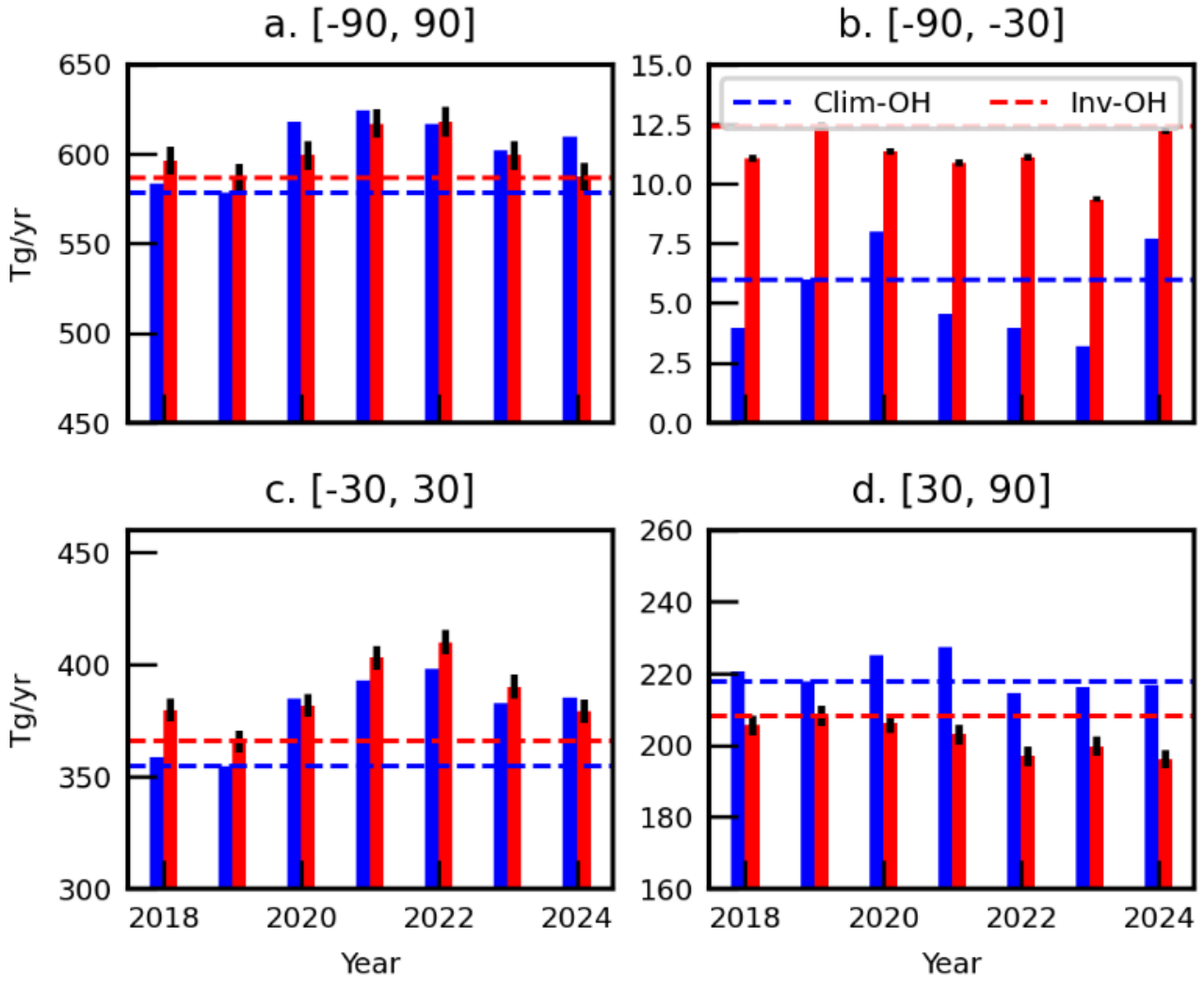

605

Figure 4: Annual mean a posteriori values for the emission of methane, 2018-2024, for Clim-OH (blue) and Inv-OH (red) inversions. Panels show results for the (**a**) globe, (**b**) southern extratropics, (**c**) tropics, and (**d**) northern extratropics. The blue and red horizontal dashed lines denote a priori values for the Clim-OH and Inv-OH inversions in 2019, respectively.

610

https://doi.org/10.5194/egusphere-2026-2662
Preprint. Discussion started: 29 May 2026

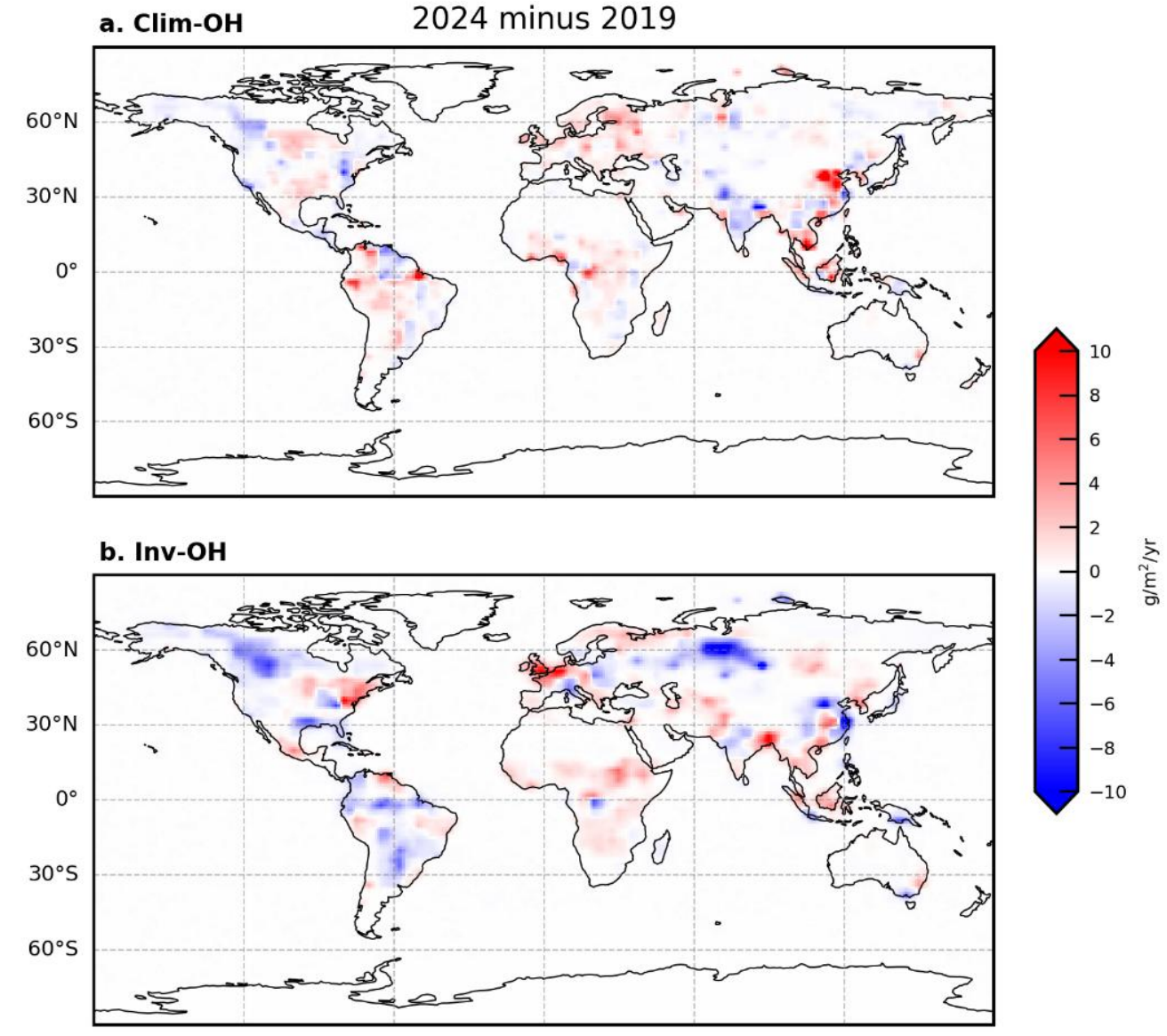

Figure 5: A posteriori annual mean spatial distribution of the difference in methane emissions due to oxidation by OH, 2024 minus 2019 for (**a)** Clim-OH and (**b**) Inv-OH inversions.

https://doi.org/10.5194/egusphere-2026-2662
Preprint. Discussion started: 29 May 2026

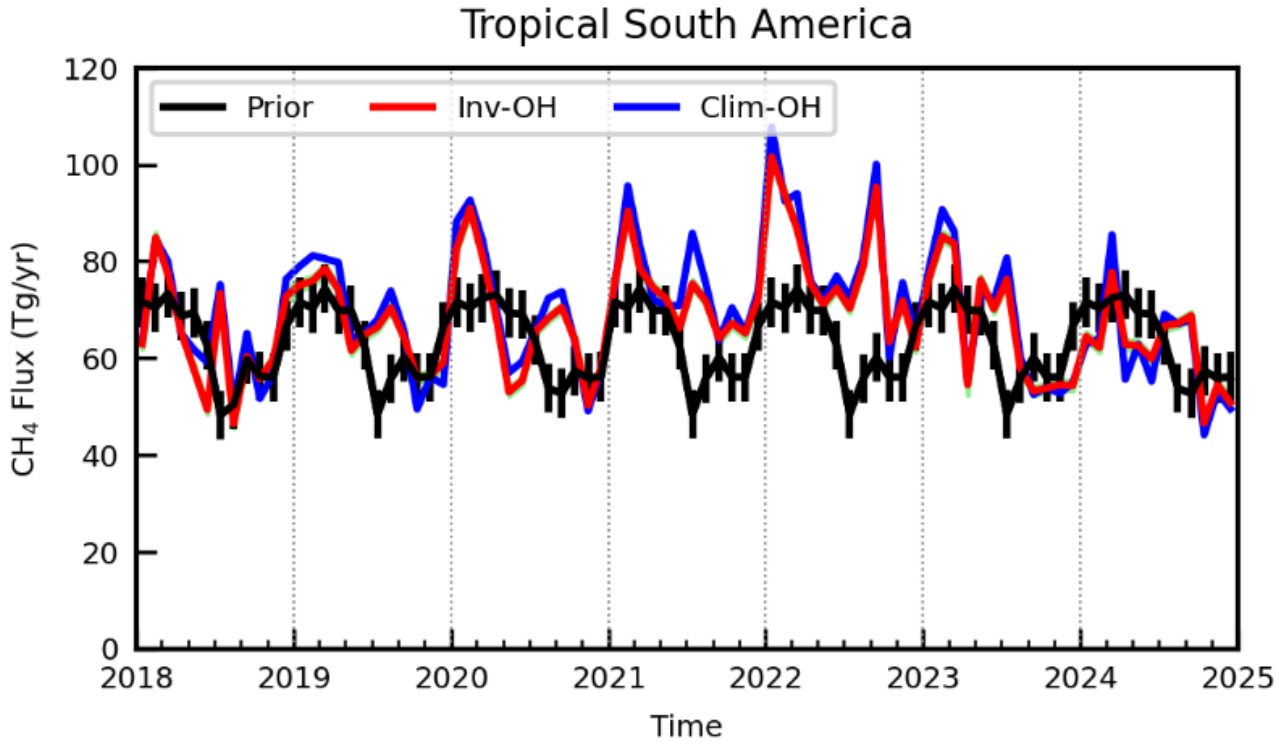

620

Figure 6: Comparison of monthly a posteriori methane emissions for tropical South America as defined in TransCom-3 for Clim-OH (blue) and Inv-OH (red) inversions. A priori values are shown by the black line

625

https://doi.org/10.5194/egusphere-2026-2662
Preprint. Discussion started: 29 May 2026

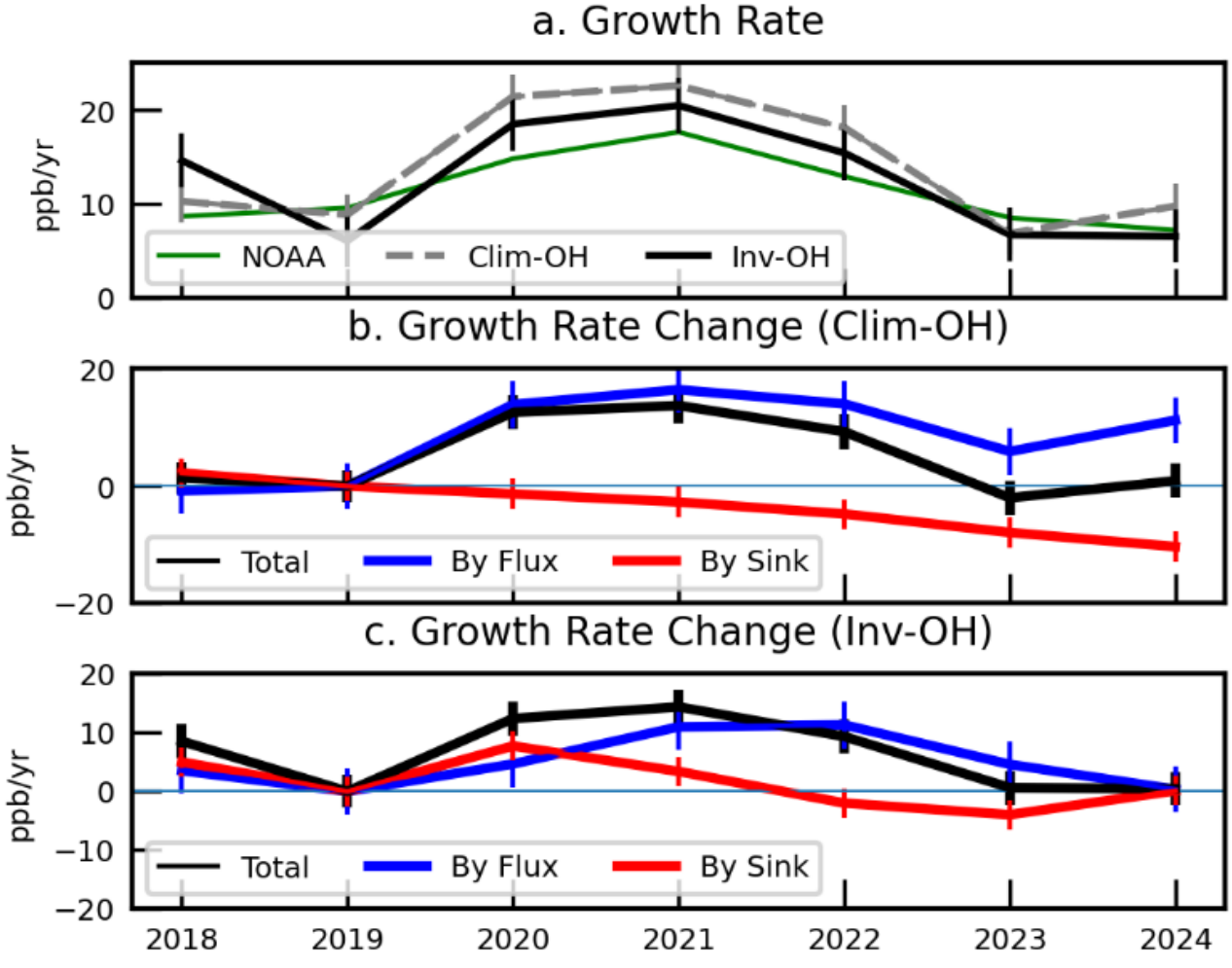

630

Figure 7: (**a)** Annual mean atmospheric growth rates inferred from NOAA data (cyan) and from a posteriori estimates from the Clim-OH (dashed) and Inv-OH (black) inversions. Contributions to the a posteriori growth rate estimates due to changes in surface emissions and changes in the chemical loss from the **(b)** Clim-OH (blue) and **(c)** Inv-OH a posteriori estimates (red). Vertical lines denote the 1-sigma uncertainty.

635

https://doi.org/10.5194/egusphere-2026-2662
Preprint. Discussion started: 29 May 2026

Appendix A: Supplementary figures

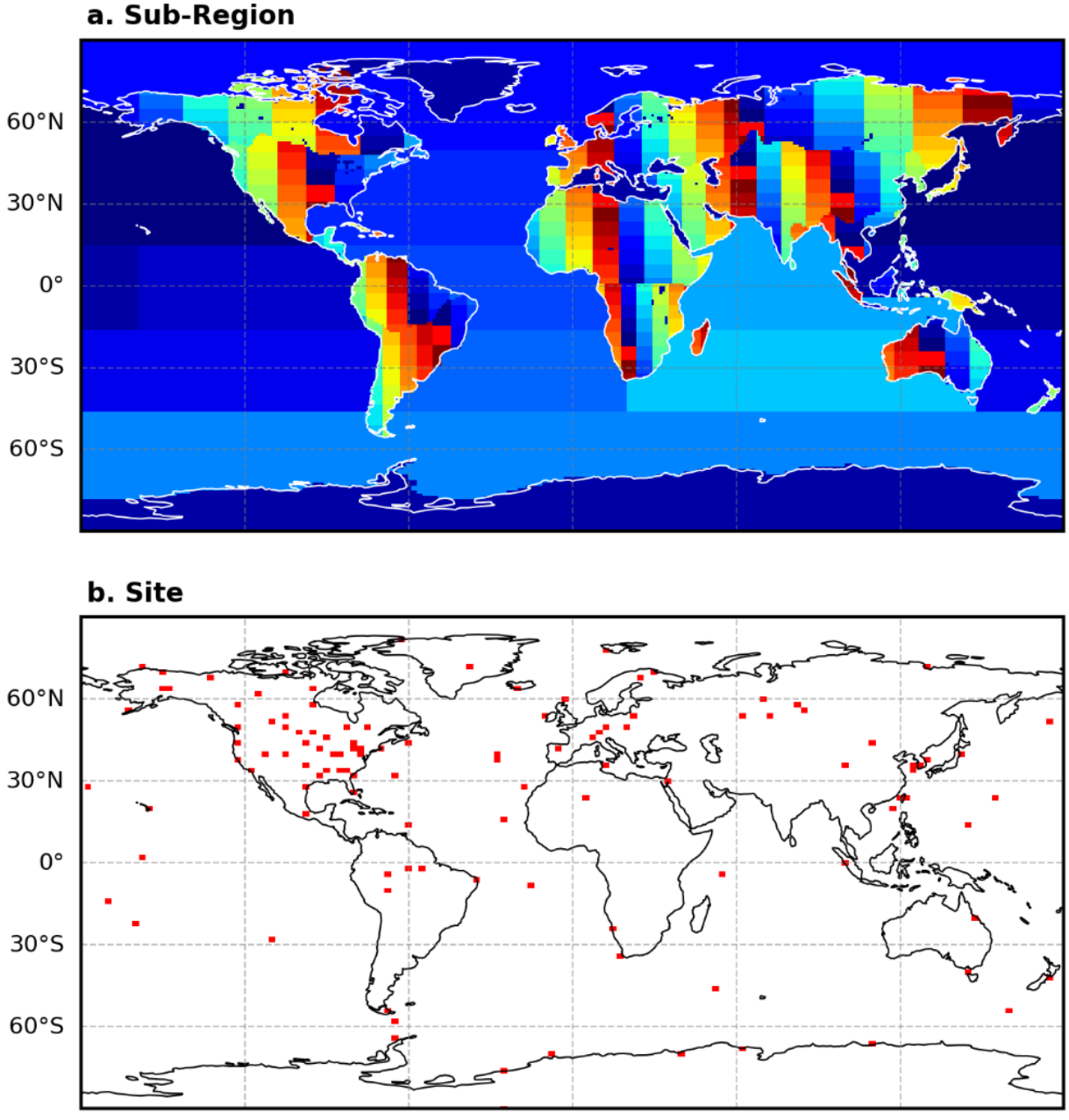

Figure A1: **(a)** Definition of sub-regions. Different colours are applied to separate neighbouring sub-regions. **(b)** Locations of the subset of in situ methane observation network

https://doi.org/10.5194/egusphere-2026-2662
Preprint. Discussion started: 29 May 2026

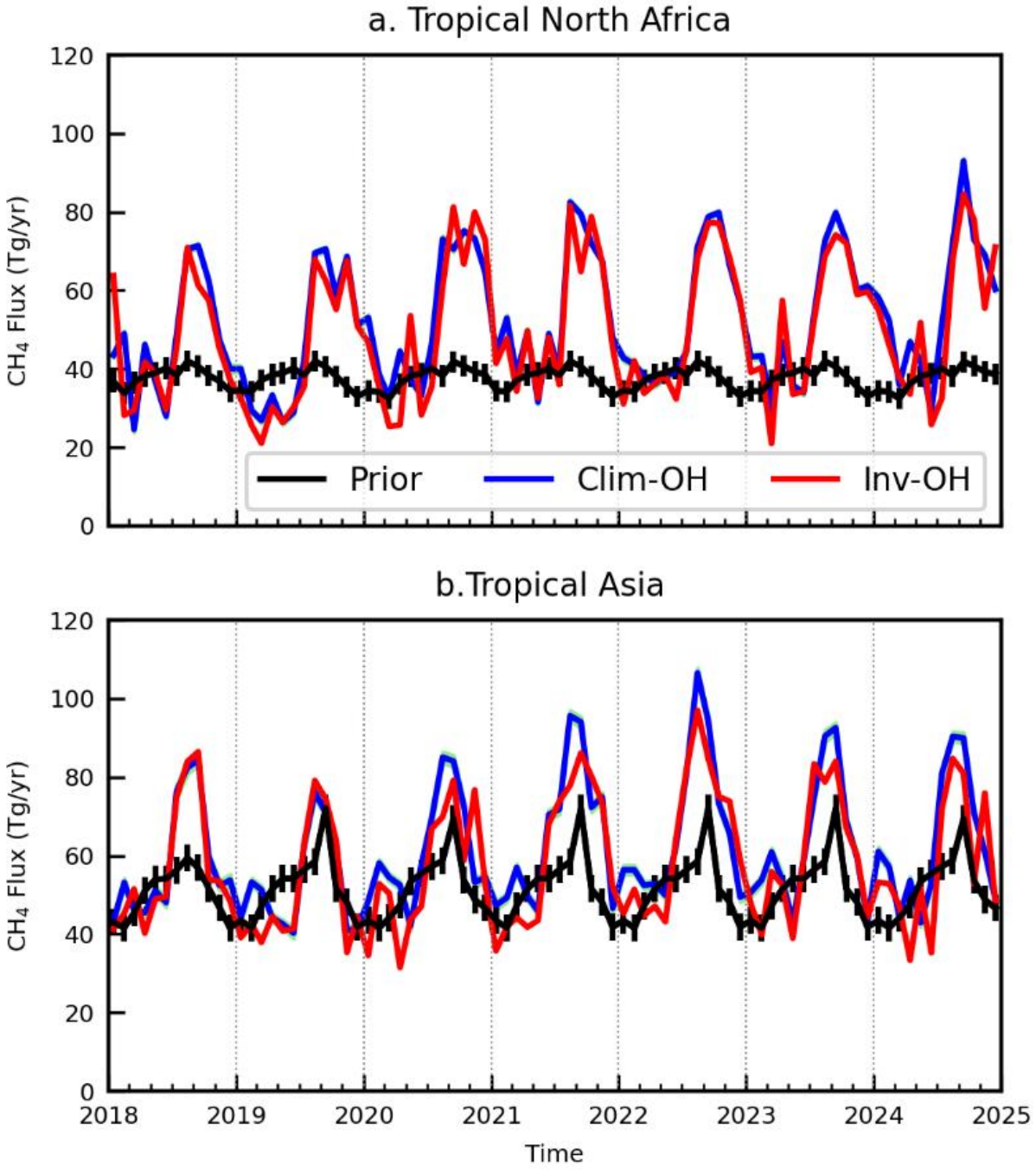

Figure A2: Same as Figure 6 but for TransCom-3 regions (**a)** Tropical North Africa and (**b**) Tropical Asia.

https://doi.org/10.5194/egusphere-2026-2662
Preprint. Discussion started: 29 May 2026

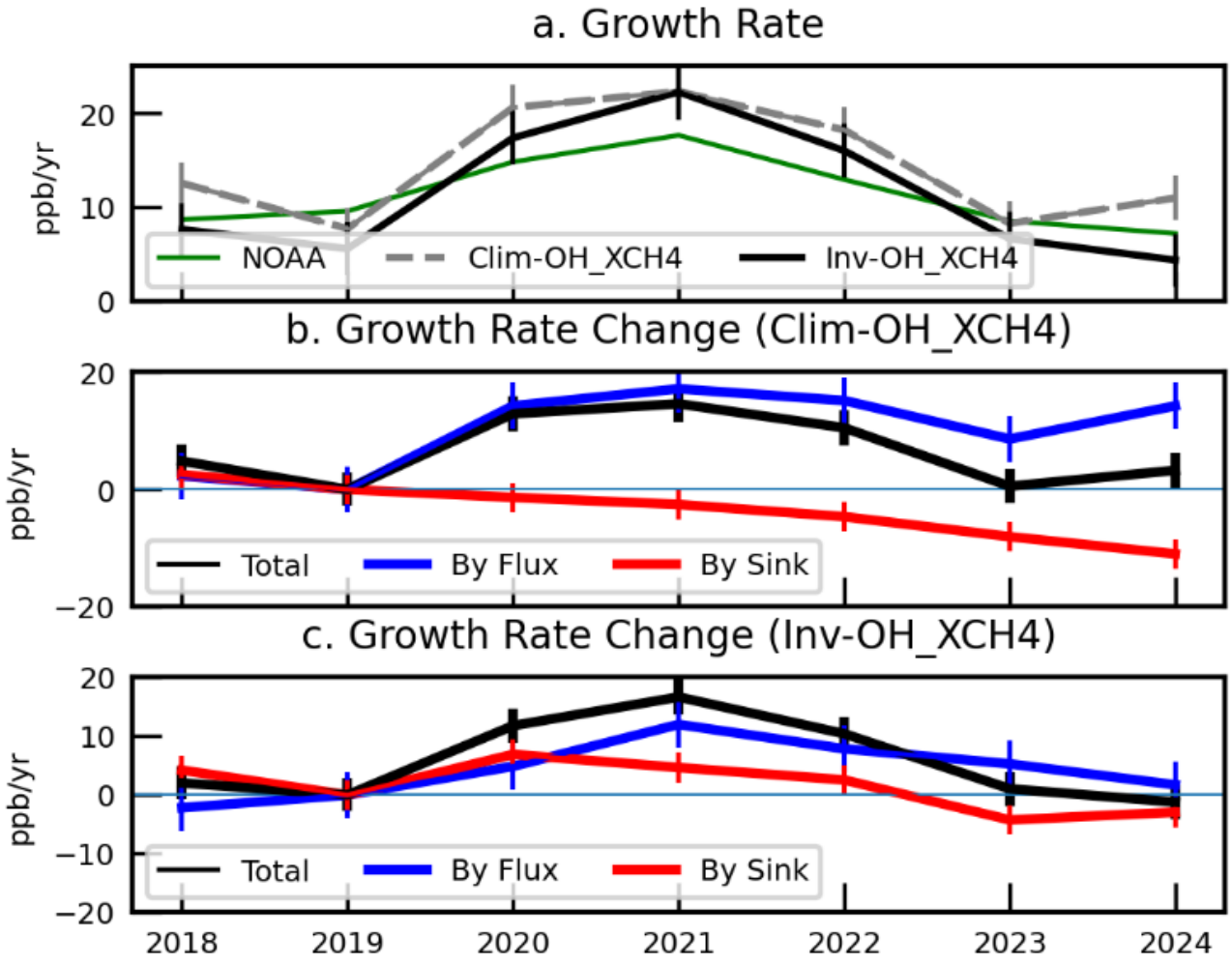

650 **Figure A3**: Same as Figure 7 but for inversions assimilating GOSAT XCH_4 retrievals only.

https://doi.org/10.5194/egusphere-2026-2662
Preprint. Discussion started: 29 May 2026

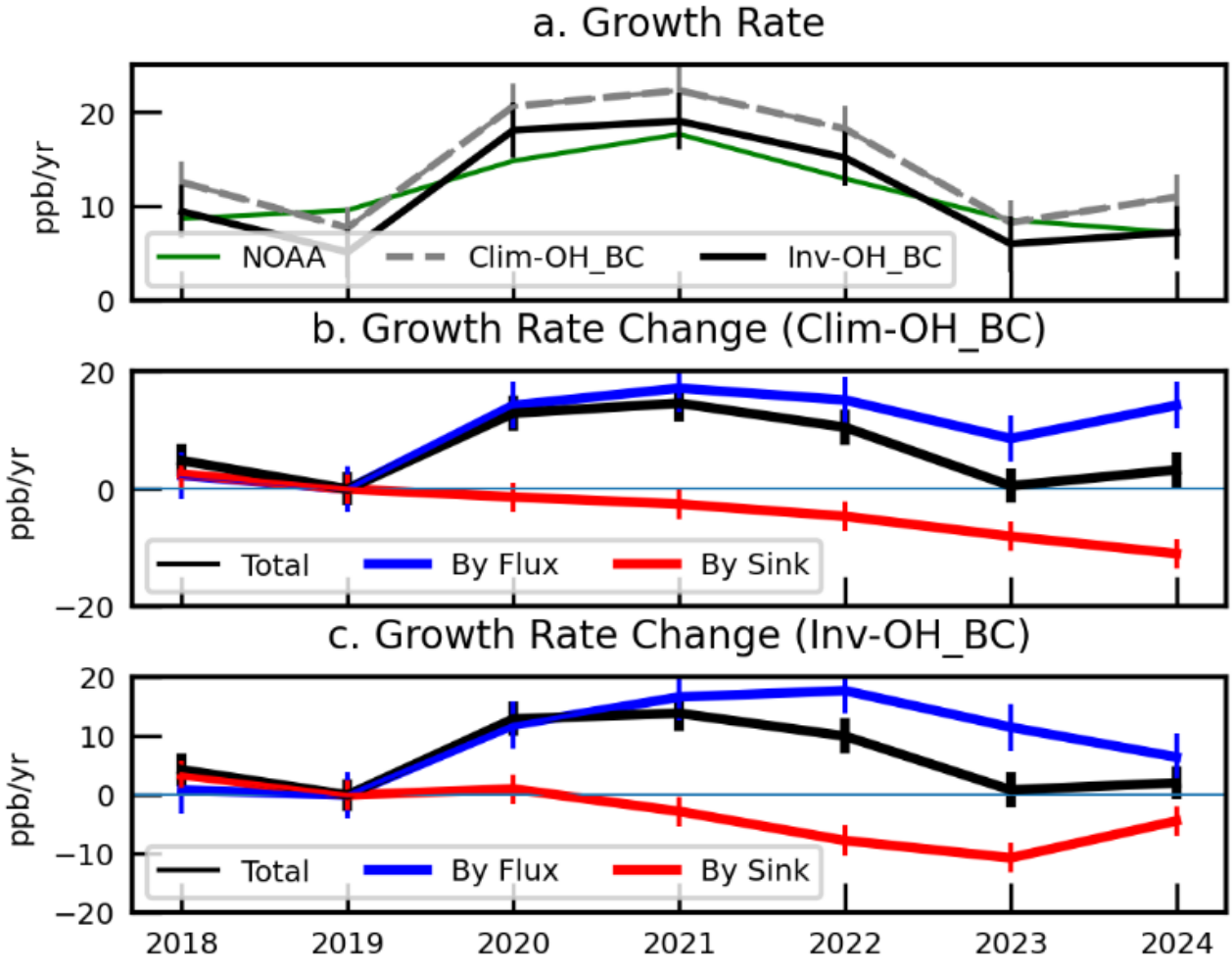

Figure A4: Same as Figure 7, but for inversions that simultaneously estimate the latitude-dependent bias by assimilating GOSAT XCH_4 and in situ observations.

https://doi.org/10.5194/egusphere-2026-2662
Preprint. Discussion started: 29 May 2026

Appendix B: Elevated loss of atmospheric methane from OH oxidation due to higher temperature

In GEOS-Chem model, and similar off-line chemical transport models, the loss rate L of OH oxidation of methane is calculated by L = [OH][methane]$k(T)$, where OH and methane denote number densities (molec/cm^2) and k denotes the temperature T (kelvin) dependent reaction rate (cm^3/molec/s).

The temperature dependent rate constant for a bimolecular reaction can be expressed using a two-parameter Arrhenius expression: $k(T) = A\ \exp(-E/RT)$, where A is the pre-exponential factor that describes how often reactive collisions occur, E denotes the activation energy that describes the minimum energy barrier that must be overcome for the reaction to proceed, and R is the universal gas constant (8.312 J/mol/K) that converts the activation energy into a temperature-scaled form so the exponent is dimensionless.

If we perturb the temperature by a small increment δT, we can describe this as:

$$exp\left(-\frac{E/R}{T}\right) = \exp\left(-\frac{E/R}{T_0+\delta T}\right) \approx \exp\left[\left(-\frac{E/R}{T_0}\right)\left(1-\frac{\delta T}{T_0}\right)\right] = \exp\left(-\frac{E/R}{T_0}\right)\exp\left(\frac{\frac{E/R}{T_0}\delta T}{T_0}\right), \quad \text{(B1)}$$

where T_0 is the reference temperature. For example, the global mean surface temperature from the MERRA2 re-analysis was about 279 K in 2019. If this temperature was 1.1K higher, (i.e. δT is about ~1.1 K) in 2024, the reaction rate , relative to 2019, k(T) increases by exp((1775/279)*(1.1/279)) ~ 2.5%, which is close to the 2.5% increase of the methane sink due to increased temperatures we report in Section 3.1. However, because the atmospheric methane OH sink is highly inhomogeneous, the 1.1 K global-mean temperature increase should be interpreted only as an effective reaction-temperature change for the whole troposphere. MERRA-2 reanalysis shows strong spatial gradients, with surface temperatures rising by 0-4 K across most mid- and low-latitude land regions but decreasing by –4-0 K over parts of the high-latitude land and ocean (**Figure B1**a), where both OH and methane concentrations are lower than over mid-latitude and tropical land. These spatially varying temperature changes translate into reaction-rate changes of roughly –10% to +10% (**Figure B1**b), underscoring the substantial temperature-driven enhancement of methane loss over several key source regions.

https://doi.org/10.5194/egusphere-2026-2662
Preprint. Discussion started: 29 May 2026

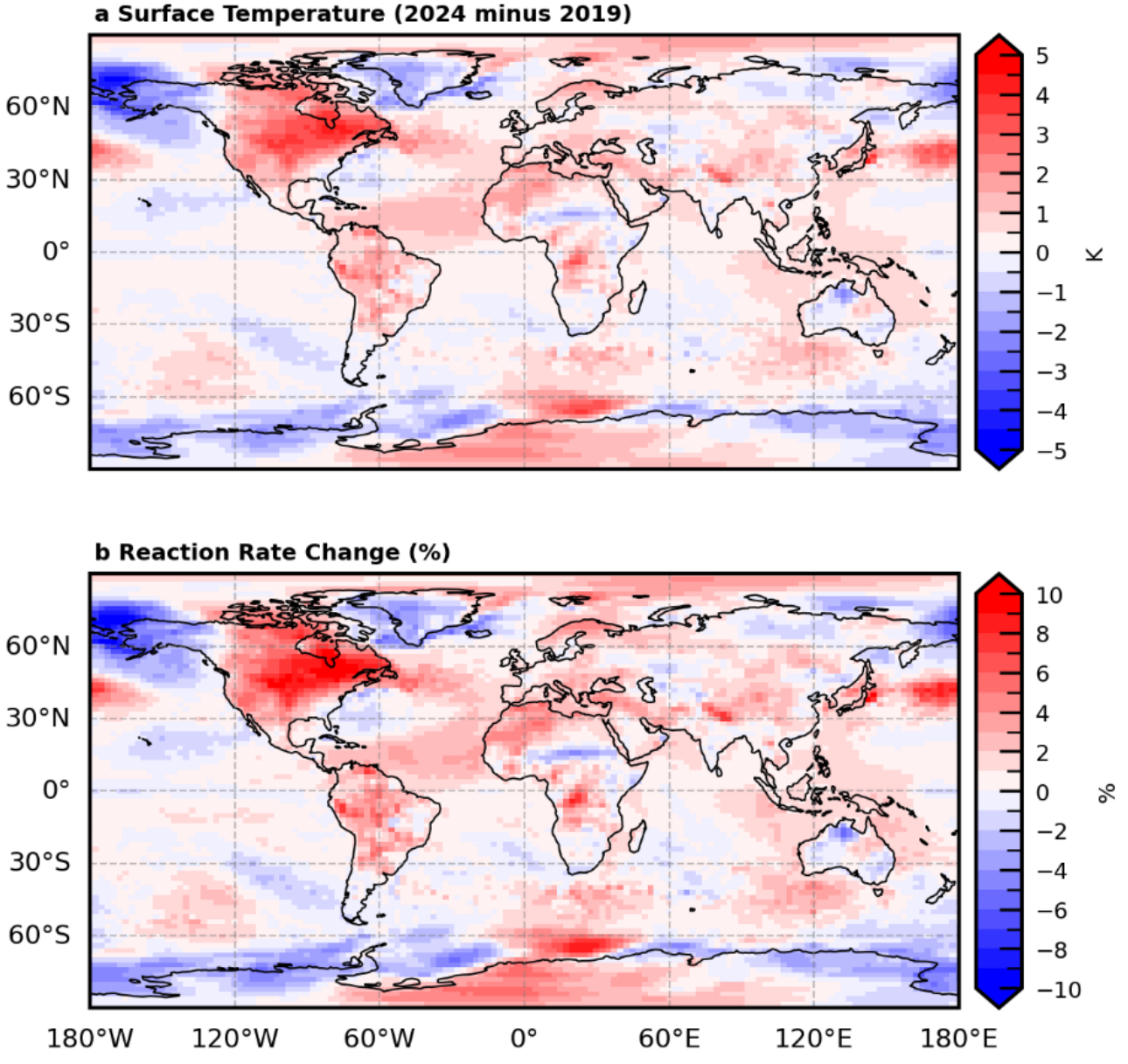

Figure B1: (**a**) MERRA2 surface temperature difference (K) between 2024 and 2019; (**b**) percentage change of the methane+OH reaction rate due to surface temperature changes, estimated using Eq. B1.